LONG-TERM FOREST GROWTH AND DECADAL SOIL CHEMISTRY CHANGE ACROSS THE WHITE MOUNTAIN NATIONAL FOREST

by

Olivia L. Fraser
B.A. Political Science, Rice University, 2007
M.S. Environmental Science and Policy, Plymouth State University, 2011

DISSERTATION

Submitted to the University of New Hampshire
in Partial Fulfillment of
the Requirements for the Degree of

Doctor of Philosophy
in
Earth and Environmental Science
September 2019

This thesis/dissertation has been examined and approved in partial fulfillment of the requirements for the degree of Doctor of Philosophy in Earth and Environmental Science by:

Dissertation Director, Mark J. Ducey, Professor (Natural Resources and the Environment)

Scott W. Bailey, Research Scientist (U.S. Forest Service)

Thomas Lee, Professor (Natural Resources and the Environment)

Mary Martin, Research Assistant Professor (Earth Systems Research Center)

Michael Palace, Associate Professor (Earth Sciences)

On January 18, 2019

Original approval signatures are on file with the University of New Hampshire Graduate School.

DEDICATION

to my parents

ACKNOWLEDGEMENTS

I would like to extend my deepest gratitude to my graduate committee, Drs. Mark Ducey, Scott Bailey, Tom Lee, Mary Martin and Michael Palace. They have shared with me much of their time and insights.

I would like to thank Steve Fay for his co-establishment of the forty permanent soil monitoring plots across the White Mountain National Forest. I would also like to thank Emily Piché, Jeff Merriam, and Ethan Belair for their assistance with field work, soil analysis, and data compilation. I would like to thank all the field crews at Bartlett Experimental Forest for the 42,070 tree measurements used in this dissertation.

Finally, I would like to thank my husband, Justin C. Fraser, for his unwavering support, and our fierce cat, Tiger Paw.

TABLE OF CONTENTS

LIST OF TABLES

LIST OF FIGURES

ABSTRACT

LONG-TERM FOREST GROWTH AND DECADAL SOIL CHEMISTRY CHANGE ACROSS THE WHITE MOUNTAIN NATIONAL FOREST

by Olivia L. Fraser
University of New Hampshire

Forest ecosystems are subject to a variety of stressors including human land use, air pollution and climate change. A challenge for detecting temporal change, however, is disentangling heterogeneity at multiple spatial scales. Therefore, we need a better understanding of the mechanisms influencing forest growth and soil formation, how to improve existing long-term sample designs, and quantify variability at multiple spatial scales. Identifying the areal extent of bedrock outcrops and shallow soils has important implications in understanding the spatial dynamics of surrounding vegetation, stream chemistry gradients, and soil properties. Manual methods of delineating bedrock outcrops and associated shallow soil are still commonly employed in the northeastern US and retain numerous limitations associated with the geometry of polygon units. Chapter 2 objectives were to assess the accuracy of visually interpreted high-resolution relief maps for locating bedrock outcrops and associated shallow soil as well as automate the delineation soil using predictive analytics. Visual interpretation of lidar-derived 1 m shaded relief maps at Hubbard Brook Experimental Forest resulted in a 92% accuracy in distinguishing the presence of bedrock outcrops and shallow soil. A generalized additive model had 88.1% overall accuracy using independent validation data and 90.1% overall accuracy predicting bedrock outcrops-shallow soil presence and absence in a second validation watershed 16 km northwest. Chapter 3 objectives were to predict the asymptotic range of stand relative density and biomass as well as explore the influence of topographic metrics as proxies for site quality. Predicting the asymptotic range of stand relative density and biomass has important implications on silvicultural practices and understanding forest carbon pools in late successional forests

across northeastern US. In addition, quantifying the influence of site quality on carrying capacity in a mixed species forest is a long-standing challenge and has not been thoroughly tested with long-term longitudinal data. Logistic and Chapman-Richards growth functions were fitted to eight decades of Bartlett Experimental Forest, New Hampshire inventory measurements from 1931-32, 1939-40, 1991-92, 2001-03, and 2015-17 as nonlinear mixed effects models. The variability associated with the plot-level random effects suggested broad differences in structure among the plots could be accounted for with topographic metrics. The variance components of predicted stand relative density and biomass asymptotes in this study influenced by a topographic covariate highlighted the importance of incorporating landscape-soil-water dynamics when characterizing stand dynamics and growth. Finally, Chapter 4 objectives were to investigate overall change in soil chemistry of mid-elevation, northern hardwood Spodosols across the White Mountain National Forest, calculate the variance components at multiple spatial scales, and stratify sampling sites by dominant hydrologic pathways to determine if groundwater influenced soils were more responsive to acidification recovery processes compared to soils developed vertically via unsaturated flow. Forty permanent plots were sampled across the White Mountain National Forest (WMNF), USA in 2001-02 and resampled in 2014. Paired t-tests detected significant increases in carbon and base cations and a decrease in Al in the Oa horizon while base cations decreased and Al increased in some mineral horizons. Additionally, within-site variability was comparable to overall variability across the WMNF. When study sites were stratified into hydrologic groups, we found a strong signal of increasing carbon and base cation concentrations from 2001-02 to 2014 for the Oa horizon, suggesting that soils influenced by shallow groundwater contributions from upslope were more responsive to acidification recovery than soils influenced only by vertical percolation. The combined approach to hydrologic stratification and estimating variance components simultaneously at the landscape and within-plot scales is crucial for calculating sample size needed to detect temporal change.

CHAPTER I

GENERAL INTRODUCTION

1.1 INTRODUCTION

This dissertation integrates forest ecology, soil science, and remote sensing methods to investigate the spatiotemporal relationships between forest growth and soil properties. The effects of 20th century acid deposition, land use, and climate change, have led to changes in soil chemistry with potentially long-term effects on soil productivity. These factors, and a lack of long-term research exploring the full breadth of various soil properties' impact on stand dynamics, have limited the adaption of silvicultural practices and management to rates of change. It is crucial to mitigate the negative impacts of forest management on soils most susceptible to change and decrease the severity of long-term impacts of anthropogenic influences in northeastern US.

Northern Forest ecosystems, along with forests elsewhere in the world, have been or are being impacted by land use change, forest harvesting, acid deposition, atmospheric CO_2 enrichment, and climate variability and change. These changes, in turn, have interacted with climatic variability and other stressors leading to reduced tree growth, episodic mortality (Long et al., 2009), and nutrient depletion from soils (Lawrence et al., 2012). This rapidly changing environment has highlighted the need for more site-specific, landscape scale forest ecosystem monitoring over short time scales (Bailey et al., 2005). Although impacts have been most obvious for nutrition-sensitive species such as red spruce (DeHayes et al., 1999) and sugar maple

(Bal et al., 2015), the effects are likely to be pervasive and persistent (Lawrence et al., 2015). Overall forest monitoring should quantify rates of change for both tree growth parameters and soil properties to best inform management practices. Therefore, this dissertation investigated spatiotemporal relationships between forest growth and soil properties as well as quantified rates of soil chemistry change.

1.1.1 Forest soil

Soils are the foundation of a forest ecosystem. Chemical properties of soils are often used as indicators of essential forest functions (Schoenholtz et al., 2000) and base cations, such as calcuim, can be used to assess forest ecosystem changes over time (Cronan and Grigal, 1995). Long-term productivity of forests depends on total amounts of available nutrients in an ecosystem (Federer et al., 1989); therefore, quantifying rates of soil change is an important component to assessing the health of forest ecosystems. Schaetzl and Thompson (2015) defined soil as the naturally occurring, three-dimensional body of organic or lithic material that has been altered by biological, chemical, and/or physical agents. Soil profile descriptions occurring at the pedon scale (1 – 10 m) are the standard for characterizing the vertical sequence of genetic soil horizons and the primary tool for classifying and mapping soils (Buol et al., 2011). The characteristics of a soil profile that are commonly described include texture, consistence, structure, color, coarse fragments, roots, and boundary (Schoeneberger, 2012). The US Soil Taxonomy system classifies soils into 12 soil orders based on dominant chemical, physical, and biological properties (Soil Survey Staff, 2014).

The five soil forming factors are parent material, climate, time, topography, and organisms (Jenny, 1941). The physical and chemical weathering of rocks and minerals at or near the Earth's

surface is a fundamental step in soil formation (Buol et al., 2011). Physical weathering causes rocks to fracture and creates additional surface area and pore space where chemical reactions can increase. Secondary minerals are formed from chemical weathering of primary minerals (Wilde, 1958) that first occurs at the exterior of surfaces of mineral particles where physical weathering increases surface area (Nezat et al., 2004). In addition, plants and their microbiota primarily contribute to the weathering by production of organic acids. Finally, parent material is important source of base cations and soils developed on glacial till could have different rates of weathering (Bailey et al., 1992). For example, Nezat et al. (2008) described the relationship between easily weathered calcium (Ca) in parent materials and exchangeable Ca in soil across northeastern United States.

1.1.2 Podzolization

Most of the Spodosols in North America formed on glacial till in cold humid climates and exist in various stages of development in the Great Lake States and northeastern United States (Hunckler and Schaetzl, 1997). Many of the soils in the forested areas of Vermont, New Hampshire, and Maine are classified as Spodosols (Figure 1.1; FAO, 2003) using the US Taxonomy criteria (FAO, 2003; Soil Survey Staff, 2014). The name “podzol” is from the Russion words “pod” and “zola” which means “under” and “ash” based on the elluvial (E) horizon created by organic (fluvic) acids leached from the O horizon (Lundström et al., 2000). The Spodosol classification criteria requires spodic materials to have a low pH, high organic carbon content, and dark spodic horizons and must have reddish or dark red colors (Soil Survey Staff, 2014), however these criteria can vary among other taxonomic systems (Lundström et al., 2000; Sauer et al., 2007). Spodic horizons have two subhorizon designations that include ‘h’

and/or ‘s’ (Soil Survey Staff, 2014; Bourgault et al., 2015). Illuvial sesquioxides include ‘s’ (e.g., Bhs, Bs) and illuvial humus include ‘h’ (e.g., Bh). Color is an important component of a soil profile description and the color of a Bhs horizon is both dark from humus and red from sesquioxides. A Bh horizon is dark from humus only and a Bs horizon is red and bright from sesquioxides only.

Figure 1.1: Areal extent of Spodosols in eastern North America (modified from FAO, 2003).

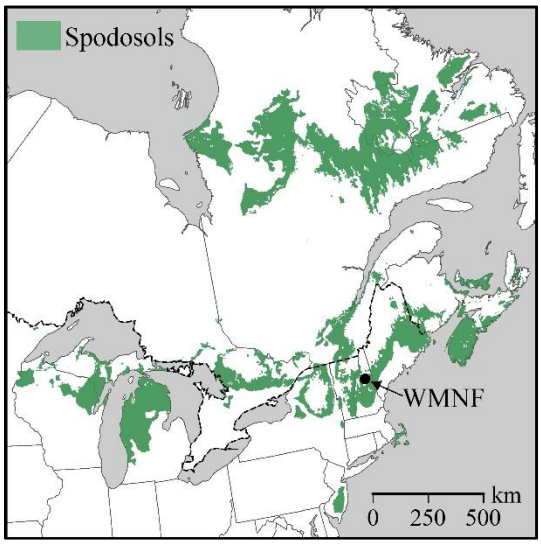

The process in which organic carbon, Fe, Al, are translocated in soil water from upper profile in the soil surface to the illuvial (B) horizon is defined as podzolization (Schaetzl, 2002). The space from the forest floor surface to the base of the B horizon is defined as the solum. Rates of podzolization are considerably different from place to place depending on parent material, soil age, water-soil dynamics, environmental factors, and past vegetative dynamics (Barrett and Schaetzl, 1998; Sommer et al., 2000). Soil processes that promote aluminum iron, and organic matter mobilization and translocation to deeper soil depths are common pathways for podzolization (Nauman et al., 2015). Depths of E horizons have been found deeper in forest

floors with increasing amounts of decaying wood in either coniferous or deciduous forests (Lundström et al., 2000). Soil forming processes operate at different spatial scales from the pedon to landscape scale, therefore it is important to consider the dominant processes of soil formation across spatial and temporal scales classifying soils.

1.1.3 Acid deposition

The human influences on sulfur (S) and nitrogen oxides emissions have drastically impacted aquatic and terrestrial ecosystems in North America during the 20th century (Rice and Herman, 2012). The acidification of the atmosphere primarily results from various industrial emissions and contributes to biological stress and degradation of ecosystem (Galloway, 1995). The Clean Air Act and Amendments of 1970 and 1990 in the United States resulted in a decrease of sulfur dioxide (SO_2) and nitrogen oxides (NO_x) emissions primarily from large industrial utilities (Driscoll et al., 2001). Despite the reduction in acidic deposition since the 1970s, more than 30 years of atmospheric transport, including SO_2, NO_x, and nitrogen (N) accumulation, has significantly modified soil chemistry and biogeochemical processes (Galloway, 1995; Likens et al., 1996; Richter and Markewitz, 2001).

Evaluating the recovery of soil properties in response to a reduction of acid deposition (DeHayes et al., 1999) is challenging and has led to numerous approaches to monitoring approaches. Repeated soil sampling is one method to detect change from acid deposition (Lawrence et al., 2013). Bailey et al. (2005) reported decreases in soil pH, exchangeable Ca, and Mg over thirty years (1967-1997) of combined Oa/A horizons in unglaciated soils in northwestern PA. Lawrence et al. (2012) observed early indications of recovery from acid deposition, increased soil pH and decrease in exchangeable Al of O horizons, from red spruce sites positioned across

northeastern US. Finally, Lawrence et al. (2015) reported decreases of exchangeable Al in the O horizon and increases in pH from O and B horizons in data compiled across 27 sites in northeastern United States and eastern Canada. It is important to fully understand the both the dominant soil forming processes and anthropogenic stressors that shape the current condition of forest soils (Wilde, 1958).

1.1.4 Forest soil monitoring

Soil quality monitoring was developed as a means of evaluating soil condition to assess the susceptibility to environmental stressors and quantify rates of change (Neary et al., 2010). Soil monitoring efforts primarily initiated in Northern forests due to increased sulfur and nitrogen deposition (Driscoll et al., 2001) associated with the depletion of exchangeable nutrient cations in soil (Likens, 2013). Properties measured often include soil solution pH because of its influence on the solubility of elements and tree growth. Calcium and magnesium are also commonly measured because they are tightly cycled between organic horizons and tree growth (Clarholm and Skyllberg, 2013).

Soil monitoring is also an essential component of informing land management decisions. However, additional sources of variability other than acid deposition, such as rates of depodzolization, contribute significant obstacles. Barrett and Schaetzl (1998) described the process of depodzolization under the removal of podzolization-promoting vegetation. Nauman et al. (2015) described how transition from conifer to deciduous forest can lose most of the organic carbon in spodosols within 100-300 years. The loss of an O and E horizon with a remnant Bs could be an indicator of past spruce influence. Prior to significant land use disturbance of the White Mountain National Forest, the areal extent of forest cover was significantly different

(Cogbill et al., 2002) and current soil properties can reveal insights in past forest composition changes. Finally, Gruba and Mulder (2015) illustrate the different effects cation exchange capacity and cation binding properties of soil organic between different tree species in acidic forest soils of southern Poland. Quantifying above- and below- ground relationships with soil production and nutrient fluxes will help adapt land management founded in a better understanding of the mechanisms causing change as a result of both soil formation and stressors.

1.1.5 Hydropedology

Water can influence soil formation along many pathways. The pathways in which water enters soil are affected by soil heterogeneity, saturation, texture, and the rates at which water enters the soil (Schaetzl and Thompson, 2015). The percolation of water through the soil profile can impact the rate of soil horizon formation and the rate of underlying parent material (Lin et al., 2005). Different measurements of slope (e.g., gradient, length) and slope elements (e.g., backslope, toe-slope) can be used as factors in determining the ways the water influences soil formation (Bailey et al., 2014). The study of hydropedology is an integrative approach for investigating these landscape-soil-water dynamics across (Lin et al., 2005).

Spatial distribution patterns of podzols in landscapes are commonly explained based on vertical processes (Sauer et al., 2007). More recent evidence, however, supports podzolization caused by lateral hydrologic flowpaths (Sommer, 2006; Gannon et al., 2014). In addition, studies describing varying illuviation-elluviation ratios could be interpreted as a combination of vertical and lateral of podzolization (Bailey et al., 2014). Sommer et al. (2001) described how podzol morphology varied with landscape position and Bailey et al. (2014) partitioned podzols of a catchment into functional groups with similar soil-forming factors based on hillslope position

(Figure 1.2). This approach to partitioning soils into hydropedological units (HPUs) is based on the dominant hydrologic pattern influencing soil development and material transfer influenced by hillslope shape and position (Bailey et al., 2014). The areal extent of HPUs and the spatial variations of hydrological and pedological properties in a central New Hampshire watershed can be delineated using different topographic indices quantifying surficial features (Gillin et al., 2015a).

Figure 1.2: Conceptual model of hydropedologic units (HPUs) in relation to hillslope position (modified from Bailey et al., 2014)

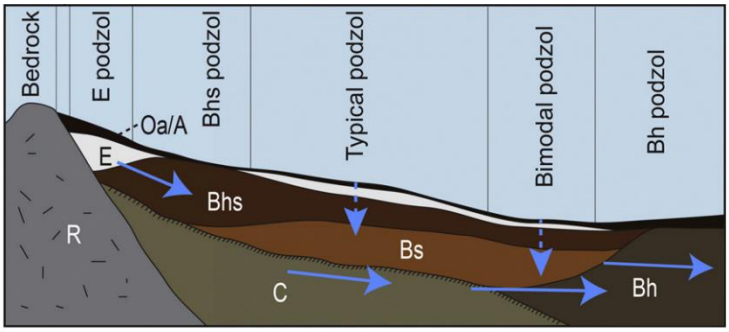

1.2 Light Detection And Ranging

Lidar, Light Detection And Ranging, is an active remote sensing technology that directly measures the three-dimensional distribution of objects by taking the product of the speed of light and the time required for an emitted laser to travel to a target object (Lefsky et al., 2002; Lim et al., 2003). The capability of an active laser scanning system, to acquire three-dimensional measurements of forest structure, has been used to estimates of the quantity and distribution of forests since the 1980s (Arp and Tranarg, 1982). Previous studies using the lidar point cloud have estimated biomass, stem volume, stand height, and stand density using lidar (Næsset, 1997;

Means et al., 1999). Additionally, common morphometric products, such as slope, aspect, and curvature, can easily be produced from a digital elevation model (DEM) created using just the lidar ground returns, however accuracy can decrease under a dense forest canopy (Su and Bork, 2006). Lidar has made it possible to generate high resolution digital elevation models (DEMs) to calculate topographic indices as a measure of the topographic control on the flow of water (Vaze et al., 2010).

Both DEM accuracy and resolution can influence the quality of DEM-derived topographic metrics (Vaze et al., 2010). For example, watershed boundaries delineated from a high resolution lidar DEM and coarse resolution contour-derived DEMs are drastically different (Gillin et al., 2015b). High resolution DEMs generated from airborne lidar use a variety of interpolation and filtering methods to separate ground and non-ground points (Guo et al., 2010) that also alter DEM-derived topographic metrics. Ashraf et al. (2012) reported the need to assess the suitability of existing algorithms for calculating slope in hydrological applications from lidar-derived DEM at different resolutions.

The four topographic metrics used to account for soil variability and map the areal extent of HPUs at Hubbard Brook Experimental Forest, NH are topographic position index (TPI), topographic wetness index (TWId), upslope accumulated flow weighted by proximity to bedrock outcrops and shallow soil (UAAb), and euclidean distance from bedrock outcrops and associated shallow soil (EDb) (Gillin et al., 2015a). Topographic position index (TPI) is calculated using the difference between the elevation of each cell and the mean elevation for a neighborhood of cells in a moving circular window with a specified radius (commonly 100 m) centered on the target cell (Guisan et al., 1999). Topographic wetness index (TWId) (Beven and Kirkby, 1979) is

computed with the upslope accumulated area (UAA) using multiple triangular flow direction algorithm (Seibert and McGlynn, 2007) as the numerator and a 5 m analysis window for downslope index (Hjerdt et al., 2004) as the denominator. Both UAAb and EDb require the delineation of bedrock outcrops and associated shallow soil. The areal extent of bedrock outcrops and associated shallow soil in the northeastern US, however, are still delineated manually (Shi et al., 2009) and retains numerous limitations associated with geometry, scale, and boundaries of polygon units (Zhu et al., 2001). It is important to incorporate these landscape-soil-water dynamics when characterizing and predicting dominant processes of soil formation and possibly an important factor in understanding the influence of soil properties on above-ground forest growth.

1.3 Stand dynamics and growth

The spatial and temporal scales in which forest ecosystems are measured and monitored are an essential factor in understanding the various mechanisms that control forest growth. The changes in total volumes of all trees or parts of trees are defined as the method for determining stand growth (Oliver and Larson, 1996). Quantifying the feedback loop between individual tree growth and evaluating overall stand growth is critical for understanding forest development (Pretzsch, 2009). An area's potential for tree growth including soil and climate conditions is referred to as the site and site productivity refers to the estimate of the site potential to produce biomass (Skovsgaard and Vanclay, 2008).

Site productivity is commonly estimated using stand age and height to define site quality (Pretzsch, 2009). The methods of assessing site productivity commonly develop site indices using height-age based relationships as an indicator of site quality (Burkhart and Tomé, 2012;

Bontemps and Bouriaud, 2014). However, this method of developing site index is commonly developed from single species and even aged stands (Skovsgaard and Vanclay, 2008). The use of these site indices in mixed species stands is challenging because the underlying assumptions of stand structure are not the same (Bontemps and Bouriaud, 2014). The challenge in developing an adequate index needs to minimize the amount of time measuring individual trees and site characteristics (Burkhart and Tomé, 2012). Another challenge is to develop an index for describing stand dynamics that can be applied at large enough scales to better understand relationships within forest ecosystems and develop meaningful management objectives (Pretzsch, 2009). Alternatively, other studies have focused on developing site index from soil properties. Hunter and Gibson (1984) showed that a height-age site index can be predicted by various soil properties (e.g., depth of A horizon) and soil chemistry in relatively young stands. McKenney and Pedlar (2003) reported jack pine height-age based site index was correlated with depth of mineral soil properties.

1.3.1 Stand density

Stand density is a measure of vegetation abundance and it is an expression of the degree of stem crowding within a stocked area as an attribute for assessing forest characteristics (Long, 1985). Stand density denotes a quantitative measurement of the stand, whereas stocking refers to the adequacy of a given stand density to meet a management object (Burkhart and Tomé, 2012). Maximum stand density, or carrying capacity, indicates the level at trees with less vigor die despite the growth of the remaining trees (Pretzsch and Biber, 2016). The number of trees per unit area, the respective tree sizes, and spatial distribution determine the extent of competition in a stand. Measure of stand density generally do not consider spatial distribution. For practical

purposes of forest management and growth and yield predication, measures of stand density strive to be 1) objective, 2) easily measured, 3) correlated with stand growth, yield, and mortality, and 4) independent of site quality (Long, 1985).

Maximum stand density is commonly defined as the maximum density that can exist for a given mean tree size in a self-thinning population (Long, 1996). In density management, maximum stand density is used to establish the upper limits of stocking assuming that site conditions are optimal (Pretzsch and Biber, 2005). Relative density is commonly defined as the density of a stand compared to maximum density (Woodall et al., 2005) and a value of 1 implies maximum density (Ducey and Knapp, 2010). Reineke (1933) and many others have asserted that maximum stand density is independent of site quality. This assumption may have resulted from the need to develop a simple mathematical index that represents so many intricate events and processes (Zeide, 2005).

Quantifying the influence of site quality on carrying capacity in a mixed species forest is a long-standing challenge. Stand relative density indices are commonly used as a stand attribute in assessments of forest characteristics and presume trees with less vigor die as live tree density increases toward carrying capacity (Burkhart and Tomé, 2012). Therefore, site occupancy is affected by stand dynamics including species composition and structure (Pretzsch, 2009). Many methods have been explored for fitting maximum size-density relationships (Burkhart and Tomé, 2012). Most notably, Reineke (1933) plotted number of trees per unit area over quadratic mean diameter on double logarithmic cross-section paper using data from fully stocked stands resulted in a straight-line relationship.

Although stand density was originally presumed to be independent of site quality, recent work supports the correlation between stand density and various environmental factors. Weiskittel et al. (2009) found that soil and climatic variables influenced the maximum density for red alder (Alnus rubra). Ducey et al. (2017) found that wood specific gravity interacts with precipitation in driving maximum density. Bravo-Oviedo et al. (2018) report that shade and drought tolerance contribute to the maximum density of a forest stand across a climatic gradient in Europe. Since the growth of a trees can be limited by the availability of light, water, nutrients, or even geometrical space (Rivoire and Moguedec, 2011), it is plausible that other site quality properties influence above ground carrying capacity or growth rate. The role of vertical or lateral hydrologic flow on the solum is well documented, however, the influence of soil-water interactions impacting stand density and forest growth is unexplored.

1.4 RESEARCH QUESTIONS AND OBJECTIVES

Therefore, the objectives of this dissertation were to 1) automate the delineation of bedrock outcrops and associated shallow soil; 2) investigate the relationship between topographic metrics as proxies for site quality with the predicted asymptote of stand relative density and biomass; and 3) quantify rates of soil chemistry change in northern hardwood forests across the White Mountain National Forest in New Hampshire and adjacent western Maine.

Objective 1 was to explore various predictive modeling approaches to delineate the areal extent of bedrock outcrops and associated shallow soils at Hubbard Brook Experimental Forest. Identifying the areal extent of bedrock outcrops and shallow soils has important implications in understanding the spatial dynamics of surrounding vegetation, stream chemistry gradients, and various soil properties. Previous studies have explored automating the delineation of bedrock

outcrops using high-resolution panoramic photographs and image classification techniques. However, image classification and topographic metrics are not universally applicable and the challenge to delineate bedrock outcrops with dense vegetation cover in the northeastern US remains. Therefore, the primary objectives were to assess the accuracy of visually interpreting high-resolution relief maps for locating bedrock outcrops and associated shallow soil as well as automate the delineation using predictive analytics.

Objective 2 was to investigate various topographic metrics as proxies for site quality in relation to the asymptote of stand relative density and biomass. Although stand density was originally presumed to be independent of site quality, recent work supports the correlation between stand density and various environmental factors. The Bartlett Experimental Forest (BEF) is approximately 1,052 ha located in the White Mountain National Forest, with elevations ranging from 200 to 900 m. Permanent plots were established in 1921-32 and re-measured in 1939-40, 1991-92, 2001-05, and 2015-17. Since the influence of site quality on stand density has not been thoroughly tested with long-term longitudinal data, the eight decades of inventory data were leveraged to explore the influence of site quality proxies on the asymptote of predicted stand relative density and biomass.

Objective 3 was to quantify the rate of change in soil chemistry of low-mid elevation, upland till soils across the White Mountain National Forest (WMNF). This required a comparison of overall changes in soil chemistry from permanent long-term monitoring plots as well as calculating within-site variance. The second objective was to stratify sampling site by dominant hydrologic pathways to determine if groundwater influenced soils were more responsive to acidification recovery processes compared to soils developed vertically via unsaturated flow.

CHAPTER 2

PREDICTIVE MODELING OF BEDROCK OUTCROPS AND SHALLOW SOIL AT HUBBARD BROOK EXPERIMENTAL FOREST, NEW HAMPSHIRE

ABSTRACT

Identifying the areal extent of bedrock outcrops and associated shallow soils has important implications in understanding spatial patterns in vegetation composition and productivity, stream chemistry gradients, and various soil properties. Few studies have automated the delineation of bedrock outcrops, and previous research has focused on methods of digital delineations in landscapes with rapidly eroding hillslopes and sparse vegetation. Manual methods of delineating bedrock outcrops and associated shallow soils are still commonly employed and are expensive to employ over broad areas and limited by geometry of polygon units. The overall objectives of this study were to assess the accuracy of visually interpreting high-resolution relief maps for locating bedrock outcrops and to automate these delineations using predictive analytics. Visual interpretation of lidar-derived 1 m shaded relief maps at Hubbard Brook Experimental Forest (HBEF) resulted in a 70% accuracy of interpreting deep soil locations and 92% accuracy in distinguishing bedrock outcrops and shallow soil. We explored four probabilistic classifications of multiple lidar-derived topographic metrics as predictive variables for bedrock outcrops and associated shallow soil presence. All four methods identified similar predictors, including slope and two topographic position indices with a 15 and 200 m circular analysis window respectively, for bedrock outcrops and associated shallow soils. Although all classifiers yielded very similar

results with little difference in interpretation, a generalized additive model had a slightly higher kappa value, indicating best accuracy in predicting the presence of bedrock outcrops and associated shallow soil, yielding 88.1% overall accuracy using independent validation data across the primary study area, and 90.1% overall accuracy in a second validation watershed.

2.1 INTRODUCTION

Bedrock is an underlying geological material in which soil forms (Jenny, 1941), whereas bedrock outcrops emerge at Earth's surface. Weathering processes of bedrock outcrops near or at the surface are drastically different than bedrock covered with substantial amounts of regolith (Buol et al., 2011). Therefore, the presence and areal extent of bedrock outcrops and shallow soil in glaciated catchments has a key role in understanding the surrounding ecology, hydrology, and soil development.

In the northeastern US, as in other regions, vegetation often reflects the physical and chemical conditions determined by dominant geomorphic processes. In this region, forest types near bedrock outcrops are commonly found to have successional stands of softwood greater than hardwood mixtures (Leak, 1982). In addition, areas dominated by bedrock outcrops limit deep percolation, forcing lateral hydrological movement of groundwater through the rooting zone (Gannon et al., 2014) controlling spatial patterns in carbon and metal sequestration in soil profiles (Sommer et al., 2001; Bailey et al., 2014; Bourgault et al., 2017). Distance from bedrock controlled-areas and proportion of bedrock outcrops in upslope drainage areas have been used to explain much of soil vertical and horizonal variability at a watershed scale (Gillin et al., 2015a). Finally, primary mineral dissolution and soil development near bedrock outcrops can explain the

spatial variation of headwater stream chemistry, setting regional background water quality characteristics (Bailey et al., in review).

Light Detection And Ranging (lidar) digital-derived data provide a unique opportunity for bedrock and surficial geologic mapping where underlying geomorphic patterns are visible despite dense vegetation cover. Bedrock outcrops are easily distinguished by the rough topographic expression along exposed ridges of upper portions of slopes with convex curvature. A high-resolution digital elevation model (DEM) can be created from the lidar ground returns and represents Earth's bare surface. Computational algorithms are often used to automate the extraction of various terrain features from lidar-DEMs (MacMillan et al., 2000; Drăguţ and Eisank, 2011). The resulting terrain features have been classified to predict a wide range of soil properties including hydrologic influences on soil formation using multinomial logistic regression in New Hampshire, US (Gillin et al., 2015a), historical extent of Spodosols using random forests in West Virginia, US (Nauman et al., 2015), soil depth with generalized additive models in Idaho, US (Tesfa et al., 2009), and digital soil mapping using support vector machines in British Columbia, Canada (Heung et al., 2016).

Extracting bedrock outcrop features, however, is especially challenging in landscapes where outcrops are scattered and in associated thin soils constituting a thin mantle over shallow bedrock, resulting in a topographically smooth signature rather than the common rough topographic expression of exposed outcrops. Since the areal extent of bedrock outcrops serves as a predictor of various biotic and abiotic properties, a few studies have explored automating the delineation of bedrock outcrops by leveraging the rough expression and slope associated with bedrock, using high-resolution panoramic photographs (DiBiase et al., 2012), and image

classification techniques (Scarpone et al., 2017). Additionally, Milodowski et al. (2015) created a roughness metric by demonstrating that the local variability of surface normal vectors can be used as a topographic signature to identify rock exposure. However, image classification and topographic metrics are not universally applicable and the challenge to delineate bedrock outcrops with dense vegetation cover in the northeastern US remains.

The first objective of this study was to assess the accuracy of visually interpreting high-resolution DEM-derived metrics for locating bedrock outcrops and shallow soil. The second objective of this study was to automate the delineation of bedrock outcrops and shallow-to-bedrock areas using predictive analytics with lidar terrain derivates as predictors. Finally, we evaluated predictive performance of four classifiers with two independent validation datasets from separate geographic locations.

2.2 METHODS

2.2.1 Study site

Hubbard Brook Experimental Forest is within the southern White Mountains of central New Hampshire, USA (43°56′N, 71°45′W) with elevation ranging from 200 to 1,000 meters above sea level and comprising the catchment draining to third-order Hubbard Brook. The climate is humid continental with annual precipitation of 140 cm and a mean stream runoff of 90 cm (A.S. Bailey et al., 2003). Soils have 0.5 m average thickness to the base of the B horizon (Likens, 2013). Northern hardwood forest dominates HBEF including *Acer saccharum* Marsh. (sugar maple), *Betula alleghaniensis* Britt. (yellow birch) and *Fagus grandifolia* Ehrh. (American beech) as dominant species in deeper soils. Shallow-to-bedrock soils are vegetated with conifer-

dominated stands composed of *Picea rubens* Sarg. (red spruce), *Abies balsamea* (L.) Mill. (balsamfir), and *Betula cordifolia* Regel (mountain white birch). The forest was selectively harvested from 1880 to 1920, damaged by a hurricane in 1938, and is relatively mature, reaching a plateau in biomass accumulation in the 1980's (Siccama et al., 2007). Bedrock in HBEF consists of mica schist and granulite of the Silurian Rangeley Formation and granitic rocks of the Devonian Kinsman pluton (Burton et al., 2000). Bedrock is poorly exposed, outcropping mostly along ridges and in some stream channels, and covered by a veneer of glacial drift ranging up to 10 m or more in thickness.

2.2.2 Sample design and visual interpretation

The terrain data were collected using an MultiPulse lidar system in 2011 (UNH GRANIT). The laser returns were recorded at an altitude of 1,158.24 m above ground level using a 30% overlap, scan angle of 27°, a nominal pulse density of 3 pulses/m^2 and a 9.25 cm vertical RMSE accuracy. The 1 m DEM was created from returns classified as representative of the ground. Shaded relief images from three illumination angles (45˚, 135˚, 345˚) were generated from the 1 m lidar-derived DEM. The HBEF watershed boundary was buffered by 200 meters to ensure the full extent of ridges were considered. Bedrock-controlled areas were estimated to represent 40% of the study area using existing geologic maps (Burton et al., 2000). Therefore 2,000 points were randomly generated to capture 50 points per category as recommended for 2.5% sampling for accuracy assessment by Congalton and Plourde (2002) (Figure 2.1). All 2,000 points were then visually interpreted as bedrock outcrop or deep soil. Visual interpretation of bedrock-controlled regions were defined as areas exhibiting a rough topographic expression where the underlying

bedrock structure was notable. Each point was initially evaluated at 1:1,000-3,000 scale and then at a 1:6000 absolute scale to consider the context of the surrounding landscape.

Figure 2.1: Shaded relief (315˚) of Hubbard Brook Experimental Forest (HBEF) buffered by 200 meters and the 2,000 randomly generated points used for visual interpretation. The figure inset depicts the location of HBEF (43°56'N, 71°45'W) marked by a five-point star within the Northeastern USA. The solid black outlines indicate the three subset catchments selected for validation of shaded relief visual interpretations.

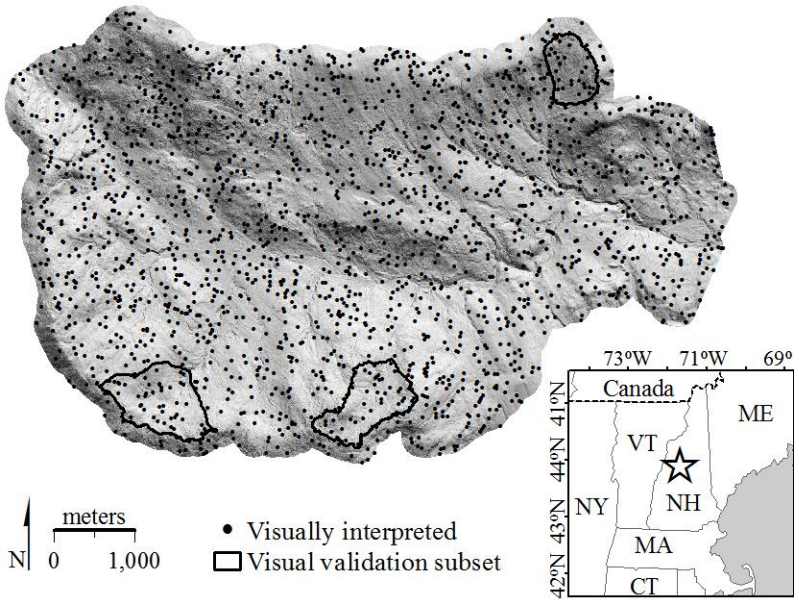

Since manual delineation is still commonly used to delineate the presence of bedrock outcrops and associated shallow soil, we validated independent visual interpretations of the high-resolution shaded relief maps. A subset of 325 points, within three catchment areas, were independently interpreted by two coauthors. One coauthor had with extensive field experience in the three subset catchments and the other did not have extensive field experience in the three

subset catchments. A total of 50 points were randomly selected from the 325 subset points for field verification.

2.2.3 Topographic metrics

A 1 m DEM was coarsened through mean cell aggregation to 5 m (Gillin et al., 2015b) and filled using an algorithm that maintains the downslope gradient (Wang and Liu, 2006). Slope (%) was calculated using the maximum slope algorithm (Travis et al., 1975). Trigonometric transformations were applied to scale aspect from -1 to 1 by combining aspect and slope according to Stage (1976). Topographic ruggedness index (TRI; Riley, 1999) was created with a 3x3 neighborhood window. Several additional vector ruggedness metrics (VRM) were created using a 3x3 and 5x5 neighborhood window size. The Zevenbergen and Thorne (1987) method was used to generate planform (PLAN) and profile (PROF) curvature. Finally, multiple topographic position indices (TPI) (Guisan et al., 1999) were created with a moving circular-window centered on a target cell using 10 m incremental sizes ranging from 5 to 250 m taking the difference between the elevation of each cell and mean elevation. A total of 11 topographic metrics were created from a 5 m DEM using RSAGA (Brenning et al., 2011) to serve as the predictor variables. RSAGA is a R package providing access to geoprocessing and terrain analysis functions of SAGA-GIS (Conrad et al., 2015). Pre-processing of the covariates was not needed since the topographic metrics explored did not exhibit multi-collinearity (Dormann et al., 2012).

2.2.4 Predictive modeling

First, a logistic regression was used to probabilistically model bedrock outcrops and shallow soil presence using independent topographic metrics. Logistic regression relates the probability of occurrence in a group to a set of predictor variables using the logit transformation (Kleinbaum et al., 2013). The outputs of logistic regression are expressed in probabilistic terms where values ranging from 0 to 1 indicate probability of occurrence, with higher values representing a higher probability. Second, we used a random forests classifier which is a hierarchical non-parametric approach that uses a combination of tree predictors and the results are based on the predictions from an ensemble of the individual trees (Breiman, 2001; Hastie et al., 2009). Each tree was trained from a randomized bootstrap sample of the entire training set and a subset of predictors randomly selected for the node-splitting rules.

We also used a generalized additive model (GAM) which is a statistical approach that generalizes multiple regression by replacing linear combinations of the explanatory variables with combinations of nonparametric smoothing or fitting functions, estimated through a back-fitting algorithms (Hastie and Tibshirani, 1990; Wood, 2004). GAM was primarily used due to flexible and smooth technique fitting either linear or non-linear predictors. Generalized cross validation criteria (GCV) was used for estimating the smoothing parameter. Finally, we used a support vector machine (SVM) approach using a linear kernel which deals with the binary classification (Hastie et al., 2009). SVM uses a hyperplane to separate the classes and predict the maximum margin of possibility between each class. In a binary classification, SVM detects the closest points between the two classes in feature space and assigns a margin based on the distance between the hyperplane and the points.

The *caret* package (Kuhn, 2008) was implemented in R (R Development Core Team) for all classifiers . The training data from the 2,000 visually interpreted points were partitioned into 5-folds for cross validation and the error rates for each of the 5 cross-validation partitions were aggregated into a mean error rate with each classifier. The accuracy of predictions were validated using the independent HBEF and WAMMO soil databases (see Section 2.4 below). Finally, the predictions of all classifiers were evaluated with the independent data using a standard error matrix (Congalton, 1991), kappa statistic (Cohen, 1960), and the significance ($p < 0.05$) of a topographic metric as an independent variable. Receiver operating characteristic (ROC) curves were created using the pROC package in R (Robin et al., 2011) by predicting the probability of occurrence with each cell in addition to a binary response. The mean probability of occurrence was calculated for the predicted presence of bedrock outcrops and shallow soil for each classifier.

2.2.5 Model validation

Two independent validation datasets were used to evaluate the predictive performance of each classifier in two different geographic areas. First, 286 pedon descriptions were used from the 412 total pedons in the HBEF soil database (Bailey, 2018) to evaluate each classifier prediction. The sample design for the independent HBEF validation database consists of pedons randomly sampled from the 431 permanent plots. The sample design consists of 15 N±S transects 500 m apart and an array of plots at 100 and 200 m distance intervals along each transect to create a geostatistical framework (Schwarz et al., 2001). The HBEF soil database includes descriptions from soil pits hand dug, approximately 0.75 x 0.5 m wide and 1.2 m deep, to sample the entire solum and the upper portion of the C horizon or bedrock, whichever comes first. Genetic

horizons were sampled and described by Munsell color, texture, structure, moist consistence, presence of redoximorphic features, rooting density, and coarse fragment content (Schoeneberger, 2012).

HBEF pedons descriptions were partitioned into by hydropedological classification (HPUs) representing the dominant hydrologic pathway influencing soil formation (Bailey et al., 2014) in order to evaluate presence or absence of bedrock outcrops. For example, Bhs podzols exhibit near instantaneous response to precipitation with a long recession period (Gannon et al., 2014). Vertical hydrologic development (typical podzol) was defined as profiles with morphology indicating a lack of watertable incursion in the solum (Gillin et al., 2015a). Lateral sites (Bh podzols) had morphology indicating regular water saturation throughout the solum while bimodal sites were intermediate with some evidence of watertable influence primarily in the lower portion of the solum (Gannon et al., 2014). Typical, bimodal, Bhs, and Bh podzols were coded as absence of bedrock outcrops and associated shallow woils. In contrast, pedons with thick Oa and E horizons and minimal B horizons overlying shallow bedrock with frequent response to precipitation were classified as O and E podzols, representative of bedrock outcrops. Figure 2 depicts representative soil profiles (plots HB035, HB051, HB125, and WS_F2) of O and E podzols from the HBEF database selected for validating presence of bedrock outcrop and shallow soil predictions. The ‘aqp’ package in R was used to create Figure 2.2 (Beaudette et al., 2013).

Figure 2.2: Representative soil profiles (plots HB035, HB051, HB125, and WS3_F2) of O and E podzols from the HBEF database selected for validating presence of bedrock outcrop and shallow soil predictions.

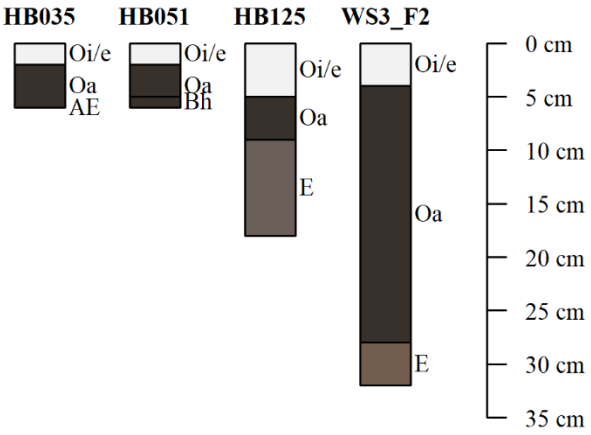

As another validation of the model, it was applied to the Wild Ammonoosuc watershed (WAMMO) 16.3 km northwest of HBEF and 181 pedon descriptions were used from the WAMMO database (U.S. Forest Service, NRM). The Wild Ammonoosuc watershed ranges in elevation from 350 to 1,350 m and contains 6,887 ha. In contrast to the HBEF soil database, the WAMMO pedon sampling design leveraged a stratified random approach based on the distribution of multiple lidar-derived topographic metrics across the watershed. This method of stratified random sampling on the WAMMO has been shown to reduce the overall prediction error since points are uniformly allocated over the feature space proportional to the distribution of the predictor (Hengl et al., 2003; Brus et al., 2011). The USDA Natural Resources Conservation Service (NRCS) described the WAMMO pedons using the same methods as HBEF (Schoeneberger, 2012). NRCS defined organic matter and bedrock-controlled soil as less than 50 cm to lithic contact. An NRCS assignment of organic matter and bedrock-controlled (ORM and

BDR) parent material category to each pedon was used to code locations as presence of bedrock outcrops and all other categories designated as absence. All locations for pedons from HBEF and WAMMO were determined using a Trimble GPS unit equipped with a Trimble Hurricane Antenna. Continuously Operating Reference Station (CORS) data from the National Geodetic Survey and Trimble Pathfinder software were used to obtain approximately 1-2 m horizontal precision after differential corrections.

2.3 RESULTS

2.3.1 Validation of visual interpretation from shaded relief maps

The independent observers who visually interpreted the 325 subset points had 91% agreement on bedrock outcrop and shallow soil locations. Areas with greatest disagreement typically occurred near a likely transition to deep soils or an isolated pocket of deep soil within an area surrounded by bedrock outcrops. Visual interpretation of shaded relief maps compared to the 51 field-verified locations yielded a 70% accuracy of interpreting deep soils and 92% accuracy in distinguishing bedrock outcrops and shallow soil (BDS). Visual interpretations of BDS presence that were in fact deep soil pockets surrounded by bedrock outcrops were also the greatest source of error.

2.3.2 Model predictions

There was very little overall difference in model results based on kappa value. The logistic regression model using slope, TPI15 (TPI with a 15 m window) and TPI200 (TPI with a 200 m window), selected by 5-fold cross validation, resulted in kappa 0.49. LR had a 75.2% accuracy predicting the visually interpreted bedrock outcrops and 81.4% accuracy predicting deep soil

locations. The LR predictions had 59.6% accuracy predicting bedrock outcrops and shallow soil presence using HBEF pedon data and 84.1% accuracy predicting deep soil locations.

The RF model resulted in kappa 0.50 with the same topographic metrics as LR. Prediction accuracy validated by the visually interpreted bedrock outcrops was 76.1% and 83.8% accuracy was achieved in predicting deep soil locations. In contrast, RF had 60.4% accuracy predicting bedrock outcrops and shallow soil presence using HBEF pedon data and 85.3 % accuracy predicting deep soil locations. The SVM model resulted in 0.51 kappa, also with the same topographic metrics, and a 61.0% accuracy predicted visually interpreted bedrock outcrops and shallow soil presence and 83.2% predicting absence.

Figure 2.3: Receiver operating characteristic (ROC) curves illustrate the binary probabilistic performance of bedrock outcrops and shallow soil presence using multinomial logistic regression (MNLR), random (RF), generalized additive models (GAM), and support vector machines (SVM).

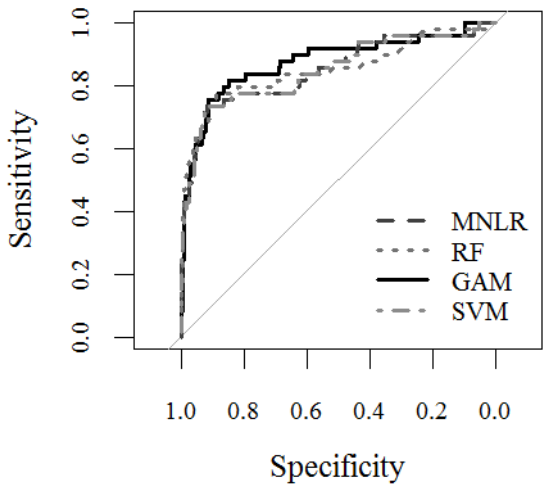

The receiver operating characteristic (ROC) curves highlight the similar accuracy results when comparing all four classifiers (Figure 2.3). However, the mean prediction probabilities for bedrock outcrops and shallow soil presence differed. The LR had a mean prediction probability of 0.62 for bedrock outcrops and shallow soil presence with a standard error (SE) of ±0.03 and RF had a mean prediction probability of 0.68 (±0.03 SE). GAM had a mean prediction probability of 0.72 for bedrock outcrops and shallow soil presence (±0.01 SE). Finally, SVM had a 0.61 mean prediction probability for bedrock outcrops and shallow soil presence (±0.03 SE). The area under the ROC curve were also very similar ranging from 0.85 to 0.86.

Figure 2.4: Different views of GAM predictions (depicted in dark grey) across HBEF displaying independent validation data using a white circle to depict deep soil sample locations and a dark grey triangle for bedrock outcrop and shallow soil sample locations.

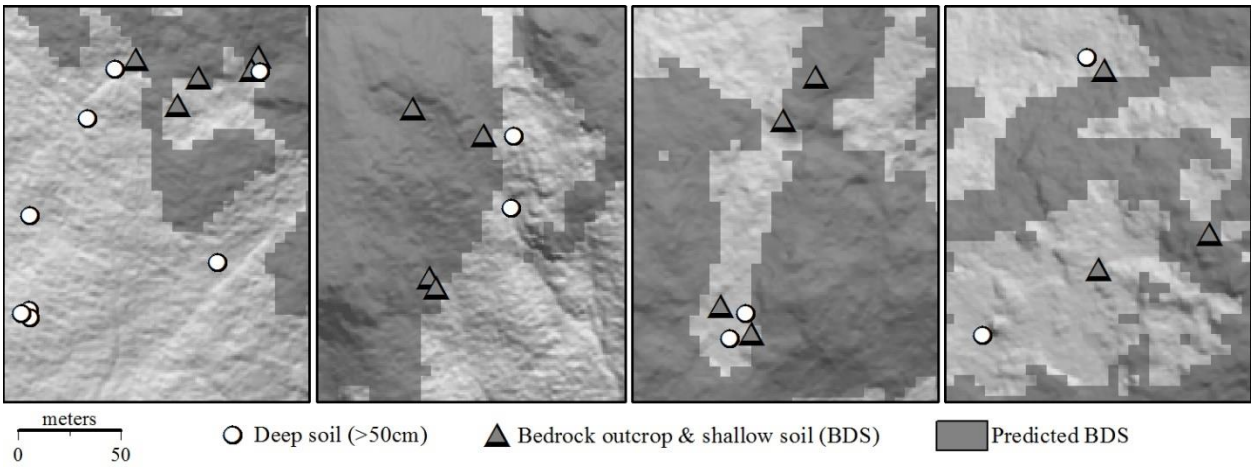

The final GAM model variables, selected by 5-fold cross validation, also included slope, TPI15 and TPI299, resulted in the highest kappa value (0.53) of all four classifiers. GAM had a 78.3% accuracy predicting the visually interpreted bedrock outcrops and 86.2% accuracy predicting deep soil locations. The GAM predictions had 63.6% accuracy predicting bedrock outcrops

presence using HBEF pedon data and 94.7% accuracy predicting deep soil locations with an overall accuracy of 88.1% (Figure 2.4). GAM applied to WAMMO had a 67.1% accuracy predicting bedrock outcrops, 95.7% accuracy predicting deep soil locations, and overall 90.4% accuracy (Supplemental Figure S2.1).

The most notable differences in classifier predictions were based on ocular comparisons. For example, LR and RF model predictions resulted in heavily pixelated predictions. Numerous bedrock outcrops and shallow soil presence pixels were randomly scattered throughout deep soil predicted locations, regardless of the probabilities. SVM and GAM predictions, however, resulted in more discrete clusters of bedrock outcrops and shallow soil presence. Single pixel predictions of bedrock outcrops-shallow presence surrounded by deep soil locations were more often predicted correctly by SVM and GAM.

The mean bottom depths of the two different classification methods from both independent validation data suggest overall agreement in identification of bedrock-controlled soil characteristics. O and E podzols at HBEF had a mean bottom depth of 33 (cm) and WAMMO pedon categorized as ORM or BDR had a mean bottom depth of 21 (cm).

2.4 DISCUSSION

Visual interpretation of terrain derivates is commonly used for mapping of bedrock geology and parent material (Haugerud et al., 2003; Belt and Paxton, 2005). Current bedrock geology and soil mapping efforts in northeastern US requires the manual delineation of bedrock-controlled areas using visual interpretation of lidar-derived hillshades (Shi et al., 2009) or derived from surficial geologic maps (McBratney et al., 2003). Since a large sample size is often required for rigorous

predictive modeling, it poses a common limitation in mapping soil, parent material, and geologic features (Hengl et al., 2003). Therefore, the visual interpretation of bedrock outcrops in this study allowed for a statistically valid sample size to be achieved with a high accuracy and agreement in identifying bedrock outcrops and shallow soil presence. The greatest source of error, in visual interpretation of lidar-derived hillshades, occurred in small pockets (< 15 m^2) of topographically smooth deep soil along ridges surrounded by bedrock outcrops and shallow soil.

Only a few studies have explored automating the delineation of bedrock outcrops. For example, Milodowski et al. (2015) created a computational algorithm for calculating a roughness metric and performed well predicting soil mantled bedrock on rapidly eroding hillslopes in California and Idaho, US. Scarpone et al. (2017) increased delineation accuracy from 48% of bedrock exposures in legacy land cover maps to 88% with the use of a random forest model using 17 predictor variables. An independent dataset, created through photo interpretation and in situ ground truthing (Sandvoss et al., 2005), was used to validate model predictions in southern British Columbia, Canada. These studies, however, occur in rapidly eroding hillslopes or areas where vegetation is sparse enough to identify bedrock outcrops from photographs and common image processing techniques of aerial imagery are applicable (Grebby et al., 2011).

Figure 2.5: Predicted bedrock outcrop-shallow soil presence in dark grey on a shaded relief map (315˚ illumination) of HBEF. Bedrock-controlled areas manually delineated are depicted by lighter grey polygons. Overall agreement on bedrock occurrence is high, however, predicted bedrock outcrop-shallow soils suggest higher presence of small pockets in the valley bottom and more scattered pockets of deep soil along the ridges.

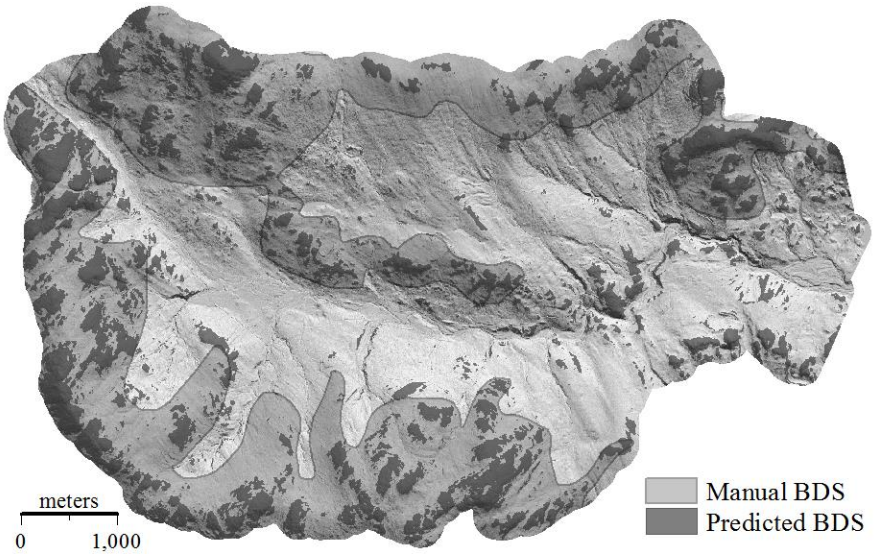

USDA Natural Resources Conservation Service (NRCS) completed a comprehensive soil parent material map across Vermont and New Hampshire generalized from detailed soil surveys and manually delineated at a 1:10,000 scale using shaded relief maps (Figure 2.5). The parent material map was validated by selective field validation to delineate polygons and determine the location of parent material transitions. The NRCS manual delineation at HBEF had a bedrock outcrops and shallow soil presence accuracy of 56% and 52% accuracy at WAMMO using the same independent validation data in this study. In comparison, the predicted bedrock outcrops and shallow soil presence using the GAM model in this study resulted in 63.6% and 67.1% accuracy at HBEF and WAMMO respectively. There is overall agreement on the topographic expression of bedrock outcrops and shallow soil interpretation high-resolution shaded relief maps as well as categorizing pedon descriptions. However, the approach to manual delineate bedrock-controlled landscape retains numerous limitations associated with the geometry, boundary, and scale of polygon units (Zhu et al., 2001). The predictive modeling approach presented in this study drastically reduces the time needed to manually delineate bedrock-controlled areas as well as increases accuracy.

The multiple radii for computing topographic position indices (TPI) in this study appears to address the challenges of topographic convexity exhibited by bedrock-controlled areas at multiple scales (Miller et al., 2015). It can be difficult to determine the radius of generating predictor variables at one specific scale, therefore, multiple window radii have the potential to produce results not limiting the scope of TPI as a predictor. Although the four classifiers in this study yielded very similar results, GAM had a slightly higher kappa value and ROC curves suggests slightly better overall binary probabilistic performance (Figure 2.3). Additive models accommodate a range of linear and smooth nonlinear effects of continuous covariates and the model process selects the most suitable covariate. In the case of bedrock outcrops, GAM results presented here highlight the nonlinear convexity of bedrock outcrops. The combination of these multi-scale covariates increases the complexity of the model to predict bedrock structure in the landscape. It is not surprising that in landscapes, such as the northeastern US with a high degree of topographic complexity, more than one neighborhood extent would be successful at characterizing pedogeomorphological processes at multiple scales.

2.5. CONCLUSIONS

Identifying the areal extent of bedrock outcrops and shallow soil in glaciated catchments has a key role in understanding the surrounding ecology, hydrology, and soil development. Extracting bedrock outcrop features, however, is especially challenging in landscapes where outcrops are scattered and in associated thin soils constituting a thin mantle over shallow bedrock. Manual methods of delineating bedrock outcrops and associated shallow soils are still commonly employed and are expensive to employ over broad areas and limited by geometry of polygon units. The overall objectives of this study were to assess the accuracy of visually interpreting high-resolution relief maps for locating bedrock outcrops and to automate these delineations

using predictive analytics. The four classifiers explored in this study yielded very similar results, however, a generalized additive model had a slightly higher kappa value and a 63.6% accuracy predicting the presence of bedrock outcrops and associated shallow soil. In comparison, manual delineation of the same study area had a 56% accuracy identifying the presence of bedrock outcrops and associated shallow soil. We were able to significantly improve the accuracy and efficiency of delineating bedrock outcrops and shallow soil presence. This study demonstrates a robust framework in which to interpret and model the multi-scale processes occurring within a landscape and likely transferable across central New Hampshire and adjacent western Maine.

CHAPTER 3

EIGHT DECADES OF STAND DENSITY AND BIOMASS IN RELATION TO TOPOGRAPHIC METRICS AT BARTLETT EXPERIMENTAL FOREST, NEW HAMPSHIRE

ABSTRACT

Predicting the asymptotic range of stand relative density and biomass has important implications on silvicultural practices and understanding forest carbon pools in late successional forests across northeastern US. Additionally, quantifying the influence of site quality on carrying capacity in a mixed species forest is a long-standing challenge and has not been thoroughly tested with long-term longitudinal data. The overall objectives of this study were to predict the asymptotic range of stand relative density and biomass as well as explore the influence of topographic metrics as proxies for site quality. Logistic and Chapman-Richards growth functions were fitted to eight decades of Bartlett Experimental Forest, New Hampshire inventory measurements from 1931-32, 1939-40, 1991-92, 2001-03, and 2015-17 as nonlinear mixed effects models. The NLME model using a Chapman-Richards growth function and asymptote as the random effect had the lowest AIC value for both stand relative density and biomass. The variability associated with the plot-level random effects suggested broad differences in structure among plots could be accounted for with topographic metric as a covariate. Both predicted asymptotes were highest on flat slopes (0-10%), south-west facing aspects, and relatively well-drained soils. These results are consistent

with expectations since topography drives hydrologic influences on soil development and forests respond to abiotic factors such as incoming solar radiation and soil moisture. However, to our knowledge this represents the first successful effort to quantify these relationships using variables that are widely available at a landscape scale

3.1 INTRODUCTION

Quantifying the influence of site quality on carrying capacity in a mixed species forest is a long-standing challenge. Relative indices are commonly used as a stand attribute in assessments of forest characteristics and presume trees with less vigor die as live tree density increases toward carrying capacity (Pretzsch, 2009). Therefore, site occupancy is affected by stand dynamics including species composition and structure. Many methods have been explored for fitting maximum size-density relationships (Burkhart and Tomé, 2012). Most notably, Reineke (1933) plotted number of trees per unit area over quadratic mean diameter on double logarithmic cross-section paper using data from fully stocked stands resulted in a straight-line relationship. These methods of establishing representative data could influence determining drivers of maximum size-density relationships.

In contrast to stand density, there are a number of variables, such as above-ground live biomass, which might be expected to change in stands over long time periods. Although Siccama et al. (2007) observed biomass plateau in northern hardwood forests at Hubbard Brook, New Hampshire, more recent studies suggest forests continue to accumulate biomass (Luyssaert et al., 2008; Keeton et al., 2011). Therefore, it is unclear which biomass model reflects regional trends in the northeastern US. Since biomass is important for understanding carbon pools (Keith et al., 2009), quantifying the late successional biomass trajectory of unmanipulated stands is crucial for

understanding the full range of management activities and, maybe, the potential for northeastern forests to serve as long-term offsetting sinks for greenhouse gas emissions.

Although stand density was originally presumed to be independent of site quality, recent work supports the correlation between stand density and various environmental factors. Weiskittel et al. (2009) found that soil and climatic variables influenced the maximum density for red alder (Alnus rubra). Ducey et al. (2017) found that wood specific gravity interacts with precipitation in driving maximum density. Bravo-Oviedo et al. (2018) report that shade and drought tolerance contribute to the maximum density of a forest stand across a climatic gradient in Europe. Since the growth of a trees can be limited by the availability of light, water, nutrients, or even geometrical space (Rivoire and Moguedec, 2011), it is plausible that other site quality properties influences above ground carrying capacity or growth rate.

Few studies have used long-term longitudinal data to explore the influence of site quality on carrying capacity. It is also difficult to collect sufficient site quality information and simultaneously quantify soil, hydrologic, and topographic properties. However, computational algorithms are often used to automate the extraction of numerous landscape features representing the site quality properties (e.g., elevation, slope, aspect) from digital elevation models (DEM), which are representative of Earth's bare surface. The advancements of deriving DEMs from lidar (Gillin et al., 2015b), improvements on calculating terrain derivates (Sørensen and Seibert, 2007), and applications of machine learning algorithms (Heung et al., 2016) have contributed to the evolution of mapping soil (Gillin et al., 2015a), water tables (Gannon et al., 2014), and bedrock-controlled landscapes (Fraser et al., 2019). Therefore, various topographic metrics derived from lidar can be used to accurately and efficiently serve as proxies for numerous site

quality properties. The influence of topographic metrics as proxies for site quality properties, such as the hydrologic influence on soil development, impacting stand relative density and biomass is unexplored.

The first objective was to predict the asymptote of stand relative density and assess the plot-level variability using long-term longitudinal data. The second object to also investigate the predicted asymptote of biomass and whether there is variability or just net change. Finally, the third object was to explore topographic metrics as a proxy for more direct measurements of site quality to determine if there are influences on rate of growth and/or asymptote on stand relative density and biomass.

3.2 METHODS

3.2.1 Study site

The study was conducted on the Bartlett Experimental Forest (BEF) (44°03'N, 71°17'W). which lies within the White Mountain National Forest in north central New Hampshire (Figure 3.1). The BEF is a 1,052 ha tract established in 1932 by the USDA Forest service. BEF is characterized as a secondary successional deciduous and coniferous forest type including northern hardwood [e.g. sugar maple (*Acer saccharum* Marsh), American beech (*Fagus grandifolia* Ehrh.), yellow birch (*Betula alleghaniensis* Britton)], red spruce-balsam fir (*Picea rubens* Sarg. – *Abies balsamea* (L.) Mill.), eastern hemlock (*Tsuga candensis* (L.) Carr.), and red oak-white pine (*Quercus rubra* L. - *Pinus strobus* L.). Soils are derived from granitic drift and tend to be coarse textured ranging from weathered shallow bedrock, outwash, compact basal till and slack-water sediments to slightly washed or heavily rinsed ablational tills (Leak, 1982). In

1931-32, approximately 450 (32 x 32 m) permanent plots, spaced approximately 200 by 100 m apart were established over the extent of the BEF. A total of 444 plots have been re-measured by 2.54 cm diameter classes and species in 1939-40, 1991-92, 2001-03, and 2015-17 of all woody stems larger than 3.8 cm diameter at breast height (DBH). The BEF has a wide range and long history of active forest manipulation and this study was conducted with 130 of 159 unmanipulated plots. A total of 20 plots had at least one inventory year missing and 9 plots exhibited drastic trends likely caused by measurement error. Stand age of unmanipulated plots range upwards of 150 years and characterized by natural forest disturbance regimes. Percent cover of conifers, northern hardwoods, and mixed species were calculated by grouping species into the three categories respectively based on the proportion of stand relative density by plot.

Figure 3.1: Shaded relief map (315˚ illumination) of Bartlett Experimental Forest (BEF) and the location of the 130 unmanipulated permanent plots with stand age ranging upward of 150 years. The inset figure depicts the location of BEF (44°03'N, 71°17'W) marked by a five-point star within the northeastern US.

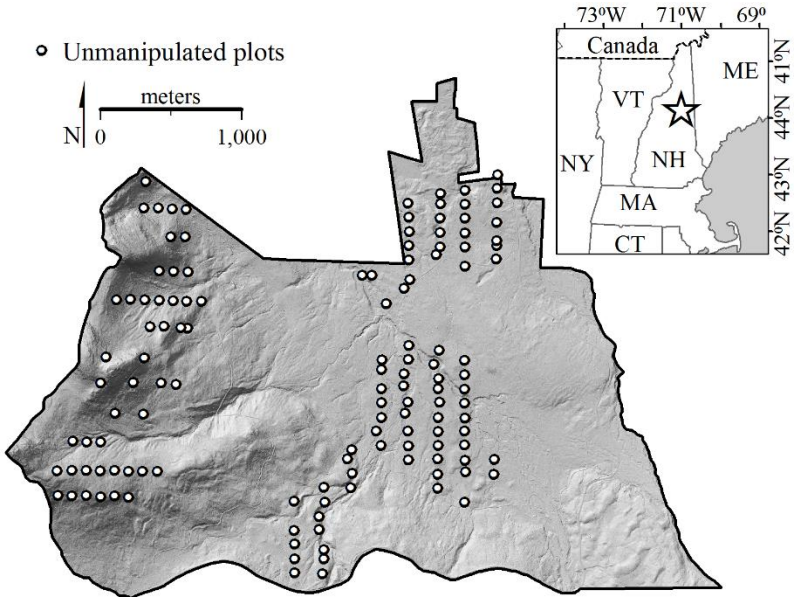

3.2.2 Statistical analysis

We fit both stand relative density (RD) and biomass to growth function commonly reported as representative of forest growth (Pretzsch, 2009; Burkhart and Tomé, 2012) as nonlinear mixed effects models. First, logistic growth (Pearl and Reed, 1920) was calculated by

$$Y = \frac{\alpha}{1+b\,\exp(-cX)} \qquad \text{[eq. 1]}$$

where y is the response variable (RD or biomass), α is the asymptote, b is half asymptote, c is scale, and X is time. In addition, Chapman-Richards function (Richards, 1959; Chapman, 1961) was calculated by

$$Y = \alpha\left(1 - \exp^{(-b1X)}\right)^{b2} \qquad \text{[eq. 2]}$$

where Y is the response variable (RD or biomass), X is time, α is the asymptote, $b1$ is the rate, and $b2$ is the y-intercept.

Ducey and Knapp (2010) was used to calculate stand relative density (eq. 3) because it accommodates a wide range of species compositions and diameter distributions. It also was developed to capture the complexity of underlying stand biology in mixed species forests in the northeastern US. Therefore, stand relative density was calculated by

$$RD = \sum_i (b_0 + b_1 SG_i)\left(\frac{DBH_i}{25}\right)^{1.6} \qquad \text{[eq. 3]}$$

where RD is stand relative density, SG_i is the mean specific gravity of trees in the stand, b_0 and b_1 are coefficients 0.00015 and 0.00218, respectively, as specified by Ducey and Knapp (2010), DBH is diameter at breast height (cm) for all live trees ≥ 12.5 cm DBH, and the summation was taken over all trees in a hectare.

Biomass was calculated using Chojnacky et al. (2014) coefficients, β_0 and β_1, because of the species updates to Jenkins et al. (2003) and the FIA approach could not be used since tree height measurements are not available for all inventory years. Therefore, biomass was calculated by

$$BM = exp(\beta_0 + \beta_1 \ln DBH) \quad \text{[eq. 4]}$$

where BM is total aboveground biomass (Mg ha^{-1}) for all live trees ≥ 12.5 cm DBH, exp is the exponential function, and ln is log base e (2.718282).

Nonlinear mixed effects (NLME) models, consisting of both fixed and random effects, were used to evaluate the variance of stand relative density and biomass asymptotes using the two nonlinear functions (Pinheiro and Bates, 2000). Random effects were specified by plot, as the grouping factor, within the mixed effects model framework to better understand overall variability compared to plot-level variability. A general expression for a nonlinear mixed effects model was specified as (e.g., Lindstrom and Bates, 1990; Pinheiro and Bates, 2000 p 282)

$$y_{ij} = f(x_{ij}, \lambda_j;\ \beta, \alpha_j) + \varepsilon_{ij} \quad \text{[eq. 3]}$$

where y_{ij} the response variable for observations of variable y from the ith plot at the jth measurement, f is a nonlinear function of predictor variable and parameter vector governing within-plot, x_{ij} is the predictor variable for observation from the ith plot at the jth measurement,

λ_j is the random-effect variable for j, β are the fixed effects parameters, α_j are the random effects parameters, and ε_{ij} is the error term.

Each growth function was fitted as a mixed effects model in R (R Development Core Team) using the *nlme* package (Pinheiro and Bates, 2000) and used the default maximum likelihood estimation. The model fits were compared using Akaike information criterion (AIC; Akaike, 1974). Models using either growth function, first examined the plot-level random effects with just α, the asymptote and then subsequent models with only one parameter as a random effect. Additional models were then explored using more than one random effect until model convergence could not be achieved. Repeated measures of forest growth typically exhibit both heteroscedasticity and autocorrelation (Gregoire, 1987). Therefore, we used a power function of the variance if the plot of the standardized residuals versus the fitted values showed within-individual error variance was heterogeneous.

3.2.3 Stand age

In order to best fit growth functions to multiple measurements over time, stand age was determined to provide a point in time representative of origin. Stand origin was used to represent 0 for both stand relative density and biomass and subsequent years were calculated by subtracting stand origin from each inventory year to provide a temporal scale. Although there is little information on the exact stand origin of permanent plots at BEF, a stand age map was created in 1929 delineating the areal extent of stands by 10, 30, 50, and 70-year age classes as well as a fifth "all-age" category. The map was digitized with a flatbed scanner and georeferenced using a 1st order polynomial (affine) transformation consisting of 4 control points (4.31 m RMSE). This resulted with 56 of the 130 plots with one of the three assigned even-age

classes, none of the plots were identified as 10 years, whereas 74 plots were described as “all-age”. Four of the 56 plots were +/- 4.31 meters of differing boundary classes and reassigned with an “all-age” category.

The younger 10 to 70-year age classes observed in 1929 were assumed to be identified correctly, however, we determined the “all-age” category represented multiple-age mixed species cohorts. Since the concept of a stratified cohort mixture did not exist in 1929 (Oliver and Larson, 1996), we concluded the 1929 observers were not identifying the “all-age” category as an alternative to uneven aged condition in older mixed species. Therefore, multinomial logistic regression was used to predict the stand age for the remaining 78 plots with an “all-age” class using the 1931 basal area (BA) and the mean DBH of the top 10 largest trees per plot as explanatory variables. Multinomial logistic regression, with 5-fold cross validation, was completed using the *caret* package in R (Kuhn, 2008). Error was assumed to be +/- 20 years since the original breaks for "even-aged" stand classes were 20 years wide. The goal was to achieve an approximation of stand origin. In order to address the lack of precise stand age, the best fitting stand relative density and biomass models were compared using +/-100 years for stand age at 10-year increments.

3.2.4 Topographic metrics

Since topographic metrics have been shown to serve as proxies for various properties of site quality, particularly soil and hydrologic properties, additional models were fit using topographic metrics as covariates. Topographic metrics were created from lidar-derived DEMs using various computational algorithms to extract terrain features. The lidar data in this study was collected during leaf-off and snow-free conditions using an MutliPulse Laser Terrain Mapper and the laser

returns were recorded at an altitude of 1,158.24 m above ground. Additionally, laser returns were recorded using a 30% overlap, a scan angle of 27°, a nominal pulse density of 3 pulses/m^2 and a 9.25 cm vertical RMSE accuracy. A 1 m DEM was created from only ground returns (GRANIT), coarsened to 5 m through mean cell aggregation and filled using an algorithm that maintains the downslope gradient (Wang and Liu, 2006). A DEM resolution of 5 m was selected because it was shown to strongly correlate with ground water fluctuations and land survey measurements (Gillin et al., 2015b).

Trigonometric transformations were applied to aspect for a -1 to 1 scale by combining aspect and slope according to Stage (1976). Slope was calculated using maximum slope algorithm (Travis et al., 1975), and both plan and profile curvature as well as a non-transformed aspect (˚) were calculated according to Zevenbergen and Thorne (1987). Topographic Ruggedness Index (TRI) was calculated by the sum difference of elevation between the subject cell and its neighbor cells (Riley, 1999). A topographic position index (TPI) was calculated using the difference between the elevation of each cell and the mean elevation for a neighborhood of cells in a 100 m moving circular window centered on the target cell (Guisan et al., 1999). Euclidean distance (m) from bedrock outcrops and associated shallow soil (EDb) was calculated using predictive modeling according to Fraser et al. (2019). Topographic wetness index (TWId) (Beven and Kirkby, 1979) was calculated with the upslope accumulated area (UAA) computed from a multiple triangular flow direction algorithm (Seibert and McGlynn, 2007) and a downslope index (Hjerdt et al., 2004) with a 5 m analysis window. All topographic metrics were calculated in RSAGA (Brenning et al. 2011) using the mean within the square plot (0.1 ha) as well as the maximum TWId value within the plot. RSAGA is a R package providing access to geoprocessing and terrain analysis functions of SAGA-GIS (Conrad et al., 2015).

3.3 RESULTS

3.3.1 Descriptive summary

The summary of forest attributes all resulted in the smallest difference between 1991-92 and 2001-03 except for biomass (Table 3.1). For example, basal area (BA) increased overall from 21.81 in 1931-32 to 38.16 in 2015-17, but the smallest difference occurred between 1991-92 and 2001-03. Quadratic mean diameter (QMD) behaved similarly, whereas stand relative density (RD) appeared to plateau between 2001-03 and 2015-17. Biomass, however, increased in relatively equal intervals between 1991-92 and 2001-03 as 2015-17.

Table 3.1: Descriptive summaries (mean and standard deviation, SD) for 130 permanent unmanipulated plots of basal area (BA), quadratic mean diametric (QMD), stand relative density (RD), biomass (Mg ha^{-1}), percent conifer (Con), northern hardwood (Nh) and mixed (Mix).

Year	BA (SD)	QMD (cm) (SD)	RD (SD)	Biomass Mg ha^{-1} (SD)	Con %	Nh %	Mix %
1931-32	21.81 (8.02)	33.97 (6.31)	0.54 (0.18)	81.01 (46.86)	20.2	62.8	17.0
1939-40	24.14 (8.09)	35.41 (6.30)	0.59 (0.17)	93.87 (53.38)	20.8	62.3	16.9
1991-92	36.06 (8.89)	40.86 (5.27)	0.80 (0.15)	146.27 (51.03)	34.4	57.8	7.9
2001-03	36.58 (9.43)	41.93 (5.25)	0.80 (0.17)	152.08 (54.04)	37.1	57.4	5.5
2015-17	38.16 (10.08)	43.58 (5.52)	0.81 (0.17)	159.28 (57.60)	42.7	53.8	3.5

Although the percent forest cover appeared to shift with an increase in conifer cover, the change was most notable in mixed species. The percent cover of northern hardwoods (Nh) remained relatively stable across the 130 permanent plots. Finally, multinomial logistic regression used to predict the stand age for the remaining 78 plots with an “all-age” class resulted in 16, 95, and 28 plots within each 30, 50, and 70-year age classes, respectively (kappa 0.52).

The mean elevation (m) of the 130 unmanipulated plots was 411.14 (Table 3.2), however the maximum elevation was 761.78 and a minimum of 225.95. The mean and standard deviation of aspect (˚) reflects a large number of plots on north-east facing slopes with a range of plots on varying degrees of steepness and roughness.

Table 3.2: Descriptive summaries (mean and standard deviation) for 130 permanent unmanipulated plots of topographic metrics used as model covariates.

Metric	mean	(SD)	Reference
DEM (m)	411.14	(160.96)	Wang and Liu (2006)
Aspect (˚)	123.85	(112.55)	Zevenbergen and Thorne (1987)
Aspect (sin)	0.15	(0.20)	Stage (1976)
Aspect (cos)	0.05	(0.16)	Stage (1976)
Slope (%)	0.28	(0.17)	Travis et al. (1975)
TRI	0.89	(0.40)	Riley (1999)
Plan	-0.01	(0.07)	Zevenbergen and Thorne (1987)
Profile	0.00	(0.01)	Zevenbergen and Thorne (1987)
TPI (100 m)	-0.39	(3.06)	Guisan et al. (1999)
EDb (m)	100.64	(104.89)	Fraser et al. (2019)
TWId	7.84	(1.39)	Seibert and McGlynn (2007)
TWId (max)	9.99	(2.50)	Seibert and McGlynn (2007)

The mean TWId and maximum TWId values showed a larger number of plots were between 6.45 and 9.23 (Figure 3.2). Fewer plots were very dry (TWId < 6.0) or extremely saturated areas (TWId > 10.0). Although plan and profile curvature indicated most plots were located on relatively flat areas, the mean TPI revealed at a larger scale (100 m) slightly more plots were located on footslopes and toeslopes (negative TPI) rather than ridge and shoulder positions (positive TPI).

Figure 3.2: Elevation (m), aspect (˚), topographic wetness index (TWId), and Euclidean distance from bedrock outcrops (EDb), used as proxies for site quality in relation to 130 permanent unmanipulated plots at Bartlett Experimental Forest (BEF).

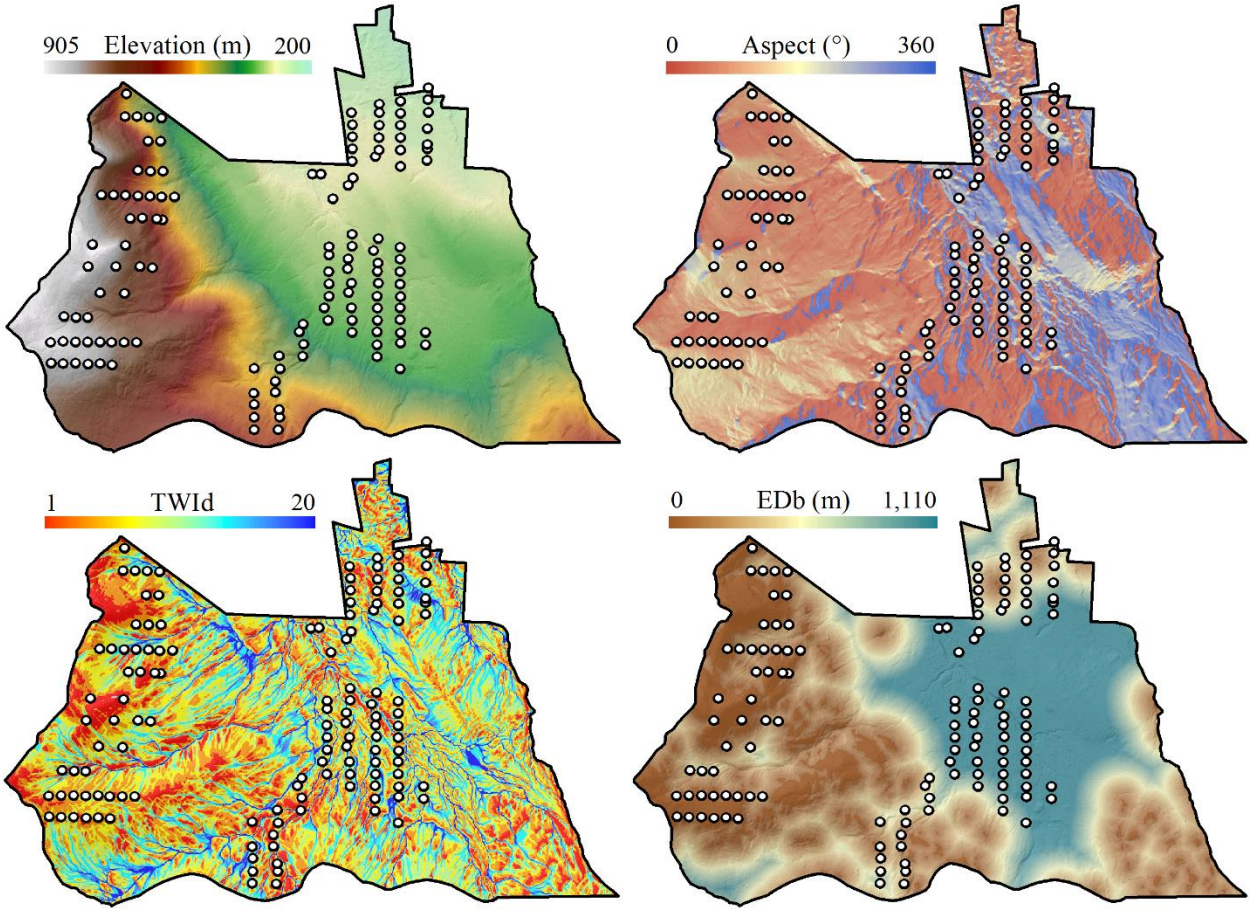

3.3.2 Stand relative density

The stand relative density model using a logistic function with the plot-level asymptote (α) as the random coefficient had a lower AIC value (-1,335.5) than the models with either the b or c as the single parameter random effect (Table 3.3). The models did not exhibit temporal autocorrelation, however, the residuals showed some inconstant variance. The variance components associated with the plot-level random effects were slightly larger than those associated with the fixed

effects. The model using the logistic function with the lowest overall AIC value had two random effects, the asymptote and b, resulting in the lowest within-plot standard error (0.054) and RMSE (0.045). Neither model exhibited temporal autocorrelation nor inconstant variance. In addition, models could not converge with a power function of the variance and correlations between variance components did not approach 1.

The stand relative density model using a Chapman-Richards function with the plot-level asymptote as the random coefficient also had a lower AIC value than other models with just one random effect, b or c (Table 3.3). The variance components associated with the plot-level random effects were also slightly larger than those associated with the fixed effects. The Chapman-Richards function resulted in the lowest AIC values with two parameter random effects, α and b1. It was the only model convergence achieved using a Chapman-Richards function with two random coefficients, α and b1. The inherent correlations between parameters in a Chapman-Richard model were evident as correlations between variance components (b1 and b2) consistently approached 1. The Chapman-Richards function resulted in a smaller AIC value (-1,734.6) than the model with the logistic function (Table 3.3).

NLME models did not have a lower AIC value using a logistic function than Chapman-Richards even when stand age was recalculated +/- 100 years using 10-year increments for each model. The NLME models had significantly lower AIC values with a logistic growth function when stand origin was 10-30 years older, however still resulted in a higher AIC value than using a Chapmen-Richards function. Stand age would have to be an additional 60 years older than all the categories provided for a logistic growth function to have a lower AIC value than Chapman-Richards.

Table 3.3: Stand relative density (RD) and biomass (BM) model results for both logistic and Chapman-Richards functions with either one or two random effects. Standard error (SE) of fixed effects, standard deviation (SD) and residual of random effects, root mean square error (RMSE), and AIC values.

Logistic										
Random effect	α	(SE)	b	(SE)	c	(SE)	random SD	2nd SD	residual	RMSE	AIC
RD α	0.80	(0.01)	43.51	(0.56)	13.82	(0.58)	0.141	-	0.083	0.076	-1335.5
RD α	0.81	(0.01)	47.35	(1.31)	10.41	(0.90)	11.263	-	0.120	0.113	-896.8
RD α	0.81	(0.01)	46.69	(0.96)	12.25	(1.11)	8.016	-	0.128	0.122	-845.5
RD α & b	0.80	(0.01)	45.56	(0.96)	11.09	(0.44)	0.152	9.497	0.054	0.045	-1619.3
RD α & c	0.80	(0.01)	47.22	(0.54)	10.94	(0.74)	0.148	6.435	0.068	0.058	-1394.4
BM α	152.95	(4.83)	49.77	(0.78)	17.66	(1.03)	53.475	-	23.100	21.190	7745.6
BM b	267.46	(9.91)	107.85	(5.04)	43.77	(2.03)	35.949	-	29.113	26.782	8057.9
BM α & b	153.82	(4.48)	55.42	(1.19)	12.20	(0.67)	50.783	12.401	15.904	13.353	7491.0
BM α & c	151.45	(4.47)	51.46	(0.51)	14.95	(1.08)	50.145	8.031	20.125	17.743	7672.8
Chapman-Richards											
Random effect	α		b1		b2		random SD	2nd SD	residual	RMSE	AIC
RD α	0.82	(0.01)	0.04	(0.003)	3.41	(0.52)	0.145	-	0.079	0.073	-1386.8
RD b1	0.84	(0.01)	0.05	(0.006)	4.22	(1.23)	0.012	-	0.120	0.142	-938.2
RD α & b1	0.83	(0.02)	0.05	(0.003)	4.06	(0.51)	0.168	0.011	0.049	0.042	-1734.6
BM α	165.09	(6.50)	0.03	(0.004)	2.26	(0.43)	57.645	-	21.895	20.074	7673.1
BM α & b1	168.85	(5.27)	0.03	(0.002)	3.32	(0.42)	49.444	0.013	14.320	13.908	7348.8

Table 3.4: NLME results for both logistic and Chapman-Richards functions with either one or two random effects and one topographic metric as a covariate. Standard error (se), standard deviation (SD) of each random effect, residuals from the random effect, root mean square error (RMSE), and AIC values.

Logistic										
Random effect(s)	α	(SE)	b	(SE)	c	(SE)	random SD	2nd SD	residual	RMSE	AIC
RD α (aspect)	0.85	(0.01)	43.58	(0.58)	13.81	(0.58)	0.124	-	0.083	0.076	-1363.6
RD b (aspect)	0.81	(0.01)	45.94	(1.12)	12.31	(1.10)	7.914	-	0.129	0.122	-847.0
RD c (aspect)	0.81	(0.01)	46.78	(0.95)	10.67	(1.29)	8.353	-	0.127	0.121	-858.4
BM α (TWId)	160.15	(5.87)	49.79	(0.78)	17.66	(1.03)	52.550	-	23.100	21.190	7743.2
BM α (EDb) & b	143.65	(5.92)	55.81	(1.64)	12.21	(0.67)	49.550	12.391	15.903	13.357	7486.1
Chapman-Richards											
Random effect(s)	α		b1		b2		random SD	2nd SD	residual	RSME	AIC
RD α (aspect)	0.87	(0.02)	0.04	(0.003)	3.43	(0.52)	0.128	-	0.079	0.073	-1414.5
RD α (aspect) & b1	0.91	(0.02)	0.04	(0.003)	3.82	(0.48)	0.136	0.010	0.049	0.042	-1789.0
BM α (aspect)	172.98	(7.54)	0.03	(0.003)	2.26	(0.43)	53.440	-	21.895	20.078	7633.6
BM α (aspect) & b1	189.08	(7.04)	0.03	(0.002)	3.61	(0.41)	51.415	14.310	14.310	12.141	7349.6

The stand relative density model using a logistic function with aspect (sin) as a covariate and only one random effect did improve model fits for asymptote or b with AIC differences of 28.1 and 12.9 respectively (Table 3.4). An approximate conditional F-test showed that aspect was significantly associated with the stand relative density asymptote ($p < 0.0101$). However, there was little improvement to the model and AIC value with just b as a random effect and any topographic covariate. Models with a logistic function, topographic covariate, and two random coefficients did not converge. The additional covariate using a Chapman-Richard function with either one or two random coefficients did, however, improved model fits by reducing AIC. The topographic metrics resulting in significant model improvements were aspect, distance from bedrock outcrops, and topographic wetness index (TWId). The model with the lowest AIC was using a Chapman-Richards function and used to predict stand relative density asymptote for each plot (Figure 3.3).

Figure 3.3: A Chapman-Richards function fitted to stand relative density (RD) and biomass for all 130 plots using the parameters from the lowest AIC model.

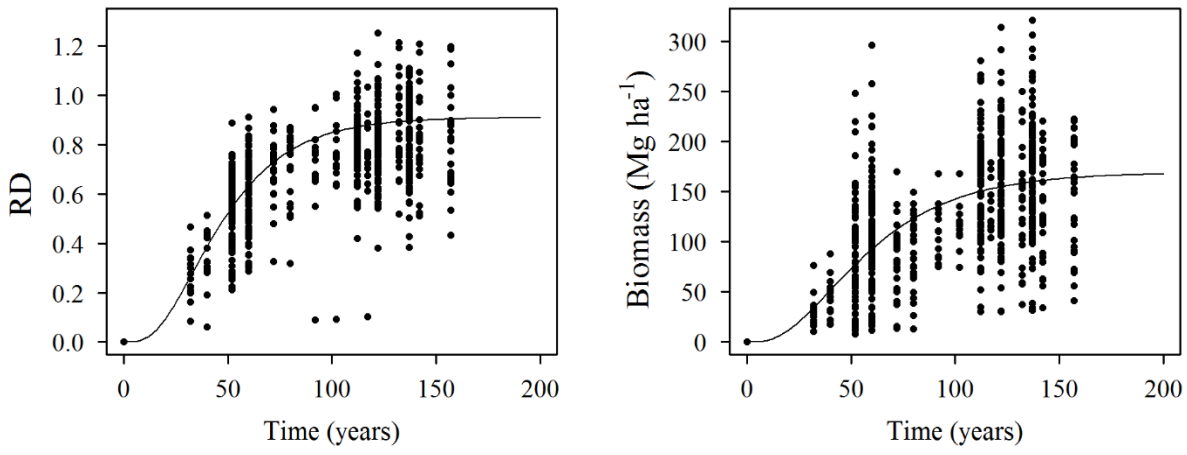

3.3.3 Biomass

Similar to stand relative density, both growth models of biomass with the plot-level asymptote as the random effect had lower AIC values than other models with one random effect, c or b (Table 3.3). The biomass model using a logistic function with the lowest AIC value overall was the model convergence achieved with two random effects using α and b. The biomass model using a Chapman-Richards function was overall a better fit, lowest AIC value, than the logistic growth function with just one random effect (7,673.09). Finally, the Chapman-Richards function resulted in the lowest AIC value with two parameter random effects, α and b1 (7,348.75).

Biomass models using a logistic function with TWId as a covariate slightly improved model fit with asymptote as the random coefficient (Table 3.4). Approximate conditional F-test also showed that TWId was significantly associated with the biomass asymptote ($p < 0.0001$). However, biomass models using a logistic function, either b or c as random effects, and a covariate did not converge. Biomass model using a logistic function with α and b as random effects with EDb as a covariate had a small AIC difference of 4.9.

The model using a Chapman-Richard function and an additional covariate with either one or two random effects had very similar AIC values (Table 3.4). The covariates that contributed overall to the most significant model improvements were aspect, distance from bedrock outcrops, and topographic wetness index (TWId). An approximate conditional F-test showed that EDb was significantly associated with the predicted biomass asymptote ($p = 0.0081$). The improvements were also notable with an additional covariate to both random effects model in the model with a Chapman-Richards function. The model using a Chapman-Richards function with the lowest AIC was used to predict the biomass asymptote for each plot (Figure 3.3).

3.4 DISCUSSION

3.4.1 Stand relative density

The asymptotic range of stand relative density is important to our understanding of stand dynamics. Few studies have collected the type of data which would provide evidence of long-term stability in stand composition and structure. Model fitting results showed the inclusion of asymptote as a random effect greatly improved all models of stand relative density. The variability (0.141-0.152) associated with the plot-level random effects suggests broad differences in structure among the plots. Therefore, the nonlinear mixed models highlighted the need to account for between-plot variation of the stand relative density asymptote. Although, the measuring protocol at BEF does not allow for individual tree growth parameters and we cannot track individual tree mortality, we can determine at the whole-stand level if the asymptote approaches 1 and goes past it.

This study also highlights the lack of BEF inventory measurements from stand origin to approximately 30 or 50 years. The results strongly suggested the best fitting model used a Chapman-Richards function and stand age would have to be an additional 60 years older in all 1929-defined categories for a model using the logistic growth function to have a lower AIC value than a Chapman-Richards function. It is unlikely the 1929 observers misidentified a 90-year old stand as 30 years or a 130-year old stand as 70 years. Additionally, the historical information regarding the BEF land use (Belcher, 1980) corroborates the 1929 stand age observations. We would gain a better understanding of growth between 30 and 50 years of stand age if BEF manipulated stand data are incorporated in the models.

Figure 3.4: The asymptote for stand relative density (RD) and biomass as predicted by the model with the lowest AIC value using a Chapman-Richards function for each plot.

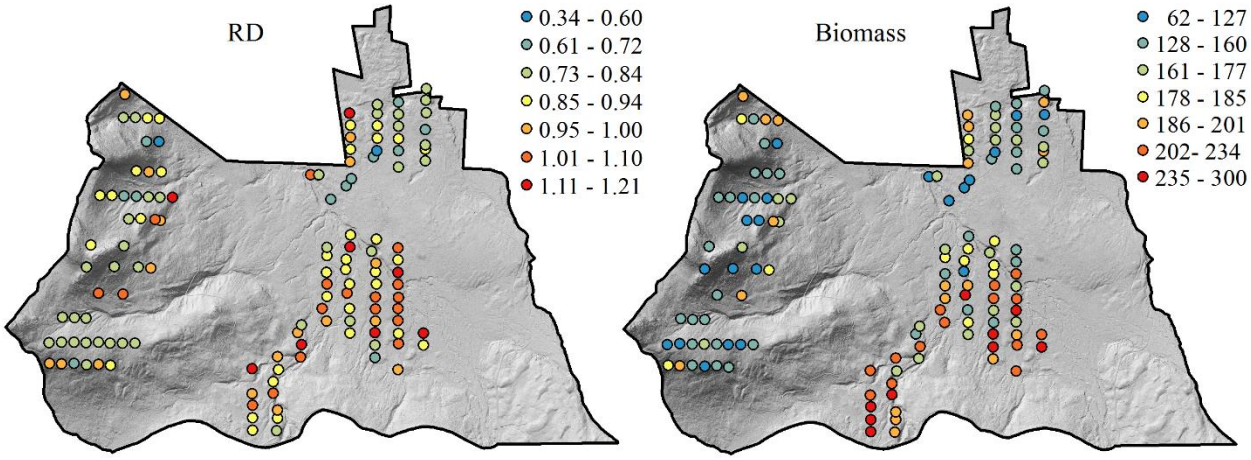

The influence of site quality on stand density has not been thoroughly tested with long-term longitudinal data. The results of a longitudinal analysis are consistent with those of static analyses of North American (Ducey et al., 2017) and European species in understanding environmental controls on stand relative density (Condés et al., 2017; Bravo-Oviedo et al., 2018). The smaller standard deviation of stand relative density (0.124-0.128) with an addition of a topographic covariate strongly suggested site quality influences the asymptote. The model using a Chapman-Richards function with the lowest AIC value was used to predict stand relative density for each plot (Figure 3.4). Aspect was significantly correlated with the predicted stand relative density asymptote ($p < 0.0101$). The predicted stand relative density asymptote was highest on relatively flat slopes (0-10%) and south-west facing aspects. For stands on steep slopes, the additive slope variable in the transformation of aspect used in this study permits the model to account for increasing slopes on more favorable aspects. The predicted stand relative density asymptote was also highest on mean TWId and maximum TWId values ranging from 7

to 8, where the B-C soil interface is saturated approximately 30-50% throughout the year (Bailey et al., 2014; Gannon et al., 2014).

These results are consistent with expectations since topography drives hydrologic flowpaths and forests respond to abiotic factors such as incoming solar radiation and soil moisture. The use of lidar-derived topographic metrics as proxies for site quality accounted for some plot-level variation and a better fitting model for each plot. The variance components of predicted stand relative density asymptote in this study using topographic covariate highlights the importance of incorporating landscape-soil-water dynamics when characterizing forest growth and stand dynamics.

The large residual variability even with a topographic covariate suggests more variation could be accounted for using other abiotic and biotic factors. For example, the proportion of Nectria fungi-damaged (Nectria coccinea var. faginata) beech (Fagus grandifolia) basal area was reported much higher on unmanipulated stands at BEF than those managed with single-tree selection (Leak, 2006). Additionally, it warrants further investigation that a larger number of unmanipulated plots are representative of lower elevations and north-east facing slopes on relatively well-drained soil to better understand the full extent of site quality on the variability of the stand relative density asymptote. Additionally, a large percentage of bedrock-controlled areas are in the western portion of BEF and predominantly northeast to east facing slopes. Although, topography appears to be critical in determining the spatial and temporal variation of forest growth at BEF, including the spatial components of permanent plots should be explored in future models.

3.4.2 Biomass

Our study also showed biomass models improved with the inclusion of asymptote as a random effect. The variability (53.48 - 57.645) associated with the plot-level random effects also suggests broad differences among the plots. Adding the random effect to the model using a Chapman-Richard function instead of a logistic function resulted in lower AIC value. The model with a topographic covariate that had a lower AIC values than a model without covariates, was the asymptote as the only random effect and slightly reduced plot-level variability. Aspect was also correlated with the predicted biomass asymptote ($p < 0.0010$).

The results in this study were consistent with previous biomass observations. The mean predicted aboveground live biomass asymptote in this study from the model with the lowest AIC value was 169 Mg ha^{-1} with a standard deviation of 49.44. The mean predicted aboveground live biomass asymptote in this study, from the model using a topographic covariate with a ΔAIC of 0.8, was 189 Mg ha^{-1} with a standard deviation of 51. The 169 and 189 Mg ha^{-1} predicted asymptotes imply that about 2.5% of sites, based on standard deviation, should show an asymptote of 267 and 290 Mg ha^{-1} respectively. Siccama et al. (2007) reported a plateau in mature northern hardwood stands of 209 Mg ha-1 on mostly south-facing slopes when stand age was estimately as 70 years at Hubbard Brook Experimental Forest, NH (Figure 3.5). The sites representative of BEF upper biomass asymptote limits, particularly those predicted with aspect as a covariate, are relatively consistent to Hubbard Brook EF observations of late successional forests on south-facing slopes. In contrast, Keeton et al. (2011) reported a prolonged logarithmic trajectory in mature and old growth northern hardwood-conifer forests across the northeastern US and the late successional forests observations were within the range of BEF. The Keeton et al. (2001) observations were representative of a much larger stand age range because it was a

chronosequence study, rather than a longitudinal study. Therefore, the differences in the two predicted asymptote trajectories were most notable between 300 and 400 years. The reported logarithmic function, however, did not represent stands younger than 100 years in comparison to BEF observations.

Figure 3.5: Biomass by stand age (years) as observed by Siccama et al. (2007) depicted in blue, Keeton et al. (2011) observations depicted in red, and BEF unmanipulated plot depicted in black. The red line represents the logarithmic function reported by Keeton et al. (2011) and the black line represents a Chapman-Richards function from this study.

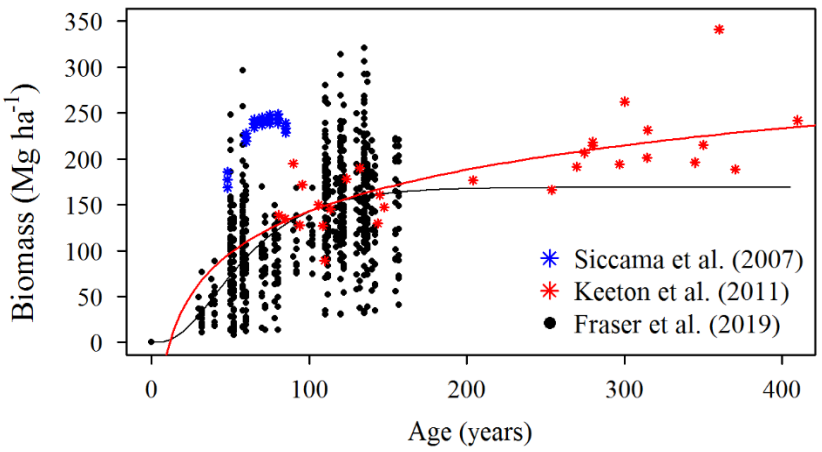

More recent studies have also reported similar biomass values, 194 Mg ha^{-1}, in late successional forests in northern Maine (Gunn et al., 2014) and ranges from 188 to 240 Mg ha^{-1} in old growth northern hardwood and softwood stands from different locations across central New Hampshire (Hoover et al., 2012). The variability in predicted asymptotes from the unmanipulated plots at BEF appears to represent the wide range of stand-level and regional biomass. Similar to stand relative density, additional environmental covariates may account for more variation and a better understanding of biomass trajectories. It is crucial for forest management practices to better

understand biomass dynamics within late successional forests as it may cover a large portion of the northeastern, US (Gunn et al., 2014). Given the complexity of secondary forest succession, it may take an additional 50 years before climax species mix is attained (Leak and Smith, 1996) and an additional 100 years to disentangle biomass accumulation trajectories of current late successional stands.

3.5 CONCLUSIONS

Forest growth models are frequently used to predict and disentangle the effects of normal successional patterns, which are often changing simultaneously. We found significant relationship between proxies of site quality and the predicted asymptote for stand relative density and possibly biomass. This study has practical implications for understanding the asymptotic range of stand relative density and biomass within individual plots and how it varies across all plots at BEF. Aspect, proximity to bedrock outcrops, and topographic wetness were found to be significant predictors in reducing within-plot variation of stand relative density. Landform, hydrologic regimes, soil characteristics and expected climax species must be considered in the management guide. These results highlight the complexity of species interactions and interactions among these factors as to which resources become more efficiently used and stand age requires further research.

CHAPTER 4

DECADAL CHANGE IN SOIL CHEMISTRY OF NORTHERN HARDWOOD FORESTS ON THE WHITE MOUNTAIN NATIONAL FOREST, NEW HAMPSHIRE, US

Chapter 4 was published as a research article in

Soil Science Society of America Journal on 012/19/2018.

ABSTRACT

Soils are subject to a variety of stressors including human land use, air pollution and climate change. A challenge for detecting temporal change is disentangling heterogeneity at multiple spatial scales. Forty permanent plots were sampled across the White Mountain National Forest (WMNF), USA in 2001-02 and resampled in 2014. Paired t-tests detected significant increases in carbon and base cations concentrations and a decrease in Al in the Oa horizon while base cations decreased and Al increased in some mineral horizons. A subset of six plots were intensively resampled in 2015. Pooled variances were calculated using all the six intensively-sampled plots from 2014-15. Within-site variability was comparable to overall variability across the WMNF. When study sites were stratified into hydrologic groups, we found a strong signal in the Oa horizon of increasing carbon and base cation concentrations from 2001-02 to 2014, suggesting that soils influenced by shallow groundwater contributions from upslope may be more responsive to acidification recovery than soils influenced only by vertical percolation. The initial study design did not consider the role of hydrologic pathways in susceptibility of soils to

temporal change and did not include enough plots in each hydrologic group to maximize the power of this stratification approach. However, these results illustrate the potential for hydrologic stratification to improve change detection and interpretation in forest soil monitoring programs. The combined approach to hydrologic stratification and estimating variance components simultaneously at the landscape and within-plot scales is crucial for calculating sample size needed to detect temporal change.

4.1 INTRODUCTION

Soils are the foundation of healthy, productive forests and their associated terrestrial and aquatic ecosystems. Long-term productivity of forests depends on amounts of available nutrients and quantifying change over time is an important component to assessing the overall health of forest ecosystems (Federer et al., 1989). Soil monitoring was developed as a means of evaluating soil condition, assessing susceptibility to environmental stressors, and informing land management practices (Mangold, 2000; Neary et al., 2010; Lawrence et al., 2013). Chemical properties of soils are monitored as indicators of essential forest functions to evaluate overall soil productivity (Cronan and Grigal, 1995; Schoenholtz et al., 2000; Richter and Markewitz, 2001). However, temporal change detection is challenging since soil chemistry is highly variable spatially and typically requires a large number of samples to achieve statistical significance (Johnson et al., 1990; Conant et al., 2003).

Soil monitoring efforts in the Northeastern US were primarily initiated due to suspected impacts of acid deposition (Driscoll et al., 2001; Likens, 2013). Studies monitoring soil chemistry change spanning between ~1967-2000, a period straddling peak atmospheric acid deposition, typically found significant decreases in Ca and significant increases in Al in the organic horizon and upper

mineral horizons (Bailey et al., 2005; Warby et al., 2009; Bedison and Johnson, 2010). However, during approximately the same time frame, Yanai et al. (1999) reported no significant change in the forest floor due to high spatial variance of Ca and Mg and a loss of 1.4% yr^{-1} would have been detectable. A more recent regional compilation of resampling efforts at 27 sites across the Northeast, comparing samples collected in the 1980s to 1990s with samples collected in the late 2000s, a period of strongly declining atmospheric acid deposition, reported signs of recovery, with modest decreases of exchangeable Al in the O and upper B horizon (Lawrence et al., 2015). However base saturation continued to decrease in the B horizon of some sites suggesting ongoing acidification. Overall soil resampling studies have varied drastically in design and few studies have investigated sampling size and study design needed to detect change across a landscape scale. Nor have there been many attempts to stratify sites by properties that could reduce spatial soil variation.

A primary challenge for soil monitoring is to disentangle heterogeneity at multiple spatial scales so variation occurring over space is not confounded with change across time. It is crucial for a monitoring protocol to account for the high variance of soil chemistry at multiple spatial scales when calculating sample size (Muukkonen et al., 2009). Often, the number of samples are determined from a site-specific perspective, which is then used as a reference for future monitoring. Previous studies have suggested sample design considerations for site-specific change detection of forest floor horizons as well as watershed scale forest floor and mineral horizon sample size (Johnson et al., 1990; Mäkipää et al., 2008). There are no long-term studies at a landscape-scale that monitored soil by leveraging a stratified sampling design based on hillslope position or other local factors driving soil formation processes to reduce the influence of horizontal and vertical variability of soil chemistry for the purposes of change detection.

Identifying site characteristics that may influence susceptibility of soil chemistry change due to acid rain or other perturbations may increase the sensitivity of monitoring programs. In the Northeastern US where Spodosols are a dominant soil order, podzolization contributes to the high-variance of soil chemistry, with eluvial and illuvial processes having greatly different expression at both the profile and hillslope scale (Bailey et al., 2014). At the profile scale, podzolization promotes translocation of soluble organic compounds, complexed with aluminum and iron, from shallow to deeper portions of soil profiles (De Coninck, 1980; Schaetzl and Harris, 2011). In addition, the dominant hydrologic pathway through a soil profile can either vertically drive leaching processes via unsaturated flow at the pedon scale, or laterally influence the leaching process, particularly in areas where shallow groundwater is flowing within the solum, connecting pedons at the hillslope scale (Lundström et al., 2000; Sommer et al., 2000; Gannon et al., 2014). Sites that are developed by vertical hydrologic flow may be more susceptible to leaching processes as buffering from atmospheric deposition and mineral weathering is limited to inputs at the pedon scale. On the other hand, sites that are developed laterally under the influence of shallow groundwater, have pedons influenced by solute inputs from upslope, with potential buffering from chemical cycling processes from a larger area than the pedon itself (Clarholm and Skyllberg, 2013). Thus these sites are potentially less susceptible to depletion processes and more responsive to recovery processes. Incorporating site characteristics to estimate the variance components simultaneously at the landscape scale, and at the profile-scale is crucial for calculating sample size and quantifying temporal rates of change when designing monitoring systems.

National forests, covering approximately 190 million acres in the US, are mandated to protect the long term soil productivity by the National Forest Management Act (NFMA, 1976). The White

Mountain National Forest (WMNF) in New Hampshire and Maine established a decadal monitoring program to measure forest soil productivity (U.S. Forest Service, 2005) to fulfill the NFMA mandate. However, it is not known how sensitive the sampling design is to detect change. The first objective of this study was to investigate overall change in soil chemistry of mid-elevation, northern hardwood Spodosols across the White Mountain National Forest (WMNF) by resampling plots that were originally sampled in 2001-02. This included further investigating temporal change detection by simultaneously calculating the variance components within-plot using a subset of plots with more intensive sampling. The second objective was to stratify sampling sites by dominant hydrologic pathways to determine if groundwater influenced soils were more responsive to acidification recovery processes compared to soils developed vertically via unsaturated flow.

4.2 METHODS

4.2.1 Study site

The White Mountain National Forest (WMNF) covers approximately 800,000 acres located in north-central New Hampshire and adjacent western Maine. Dominant vegetation types include northern hardwood, spruce-fir, and mixed-species forests. Annual precipitation averages 90-180 cm and total annual snowfall ranges from 250-400 cm (McNab and Avers, 1994). The WMNF is a glacially scoured, irregular highland characterized by clusters of low, rounded and scattered mountains where the soils are typically less than 3 m deep, strongly acid, and consist of Haplorthods, Haplaquepts, and Dystrochrepts (McNab and Avers, 1994). Figure 4.1 depicts the forty permanent plot locations across the White Mountain National Forest (WMNF) established in 2001-02 to monitor soil productivity (U.S. Forest Service, 2005).

Figure 4.1: White Mountain National Forest (WMNF) location within the northeastern US and the forty permanent plot locations established in 2001-02 across the WMNF. Each general study area is indicated by a two letter abbreviation; numbers indicate the number of plots in each general area, which ranged from one to four. In 2014, plots were sampled at 2 m intervals along topographic contour (depicted with a triangle in the magnified plot inset). A subset of 6 plots, depicted with diamonds on the WMNF map, was randomly selected for additional intensive sampling in 2015. The additional pits were sampled 2 m on contour on each side of the 2014 pit and 2 m upslope and downslope (depicted with pentagons in the plot inset) for a total of four pits sampled in the intensive plots in 2015.

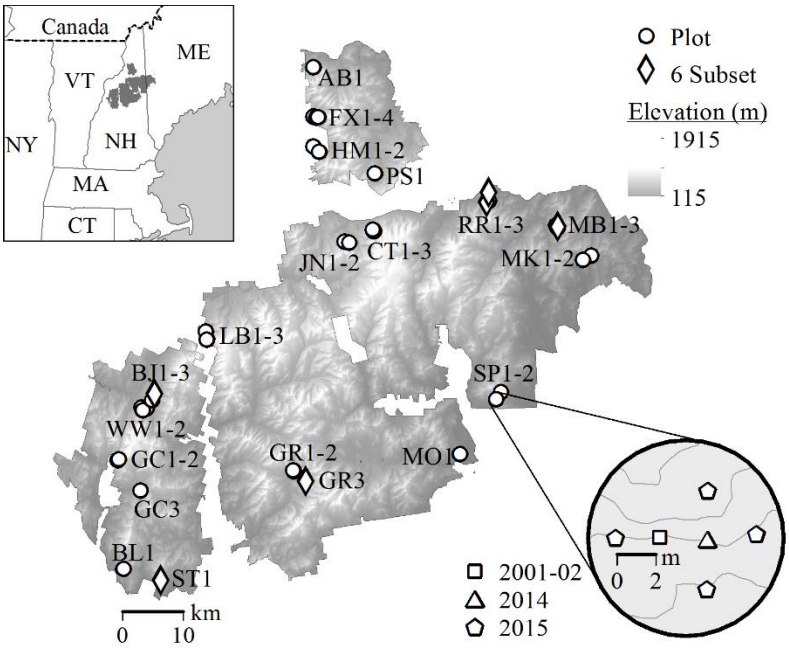

Plot locations were selected to be representative of mid-elevation mature northern hardwoods (between 60 and 120 years of age), Spodosols developed in deep glacial till, and varying hillslope position (Supplemental Table S4.1). Topographic maps, aerial imagery, and Ecological Land Types (U.S. Forest Service, 2005) were used to initially to identify locations and ensure

plots were spatially distributed across the WMNF. The focus was on mid-elevation, mature northern hardwoods since this is the portion of the WMNF most actively managed for timber products where maintenance of site productivity directly informs the achievement of goals set out in the WMNF Forest Management Plan.

4.2.2 Sample collection and analysis

Once the plots were established, aspect was measured with a handheld compass in degrees relative to true north. Slope was measured in percent with a clinometer in both up and downslope directions 5 m from plot center. Soil pits were hand dug, approximately 0.75 x 0.5 m wide and 1.2 m deep to sample the entire solum and the upper portion of the C horizon. In 2001-02, soil pits were hand dug at plot center; in 2014 plots were relocated and 37 plots were resampled. Of the 40 original plots, two plots could not be relocated in 2014 due to incorrect coordinates and one plot was resampled but classified as an Inceptisol rather than a Spodosol which was the focus of the study; these plots were excluded from the analysis presented here. In 2014 new pits were installed and sampled along the topographic contour from the plot center of the 2001-02 pit (Figure 4.1). A subset of 6 plots were selected for additional intensive sampling by stratifying all the plots based on exchangeable Al concentration. In each of the Oa, spodic (Bhs, Bh, Bs), and transitional (BC, CB) horizons, exchangeable Al concentration was classified as low, medium or high based on the entire range measured in that horizon. Two plots from each of the three categories were randomly selected for further sampling in 2015; additional pits were 2 m on topographic contour in both directions from the plot center of the 2001-02 pit and from the 2014 pit, as well as 2 m upslope and downslope of the 2014 soil pit (Figure 4.1 magnified plot inset).

Genetic horizons were described and sampled by Munsell color, texture, structure, moist consistence, presence of redoximorphic features, rooting density, and coarse fragment content (Schoeneberger, 2012). Soil samples, consisting of approximately 2-3 liters of each horizon, were collected by the full height of the horizon and width of the pit. Volumetric coarse fragment (2 mm–75 mm) content was estimated visually on the pit face. Rooting density was described semi-quantitatively as few (<1), common (1 to 5) or many (≥5) fine and very fine roots (≤2 mm in diameter) per square centimeter. B horizon subdivisions were designated based on Munsell color based on criteria shown to distinguish spodic horizons influenced by shallow groundwater at the nearby Hubbard Brook Experimental Forest (Bailey et al., 2014). Bhs horizons had a Munsell hue of 7.5YR or redder and value and chroma ≤3. Bs horizons were a 7.5YR or redder hue and a value or chroma >3 and Bh horizons had a hue of 10YR and a value and chroma both <3 (Bourgault et al., 2015).

All samples were air-dried, sieved to remove particles >2 mm, homogenized and split to generate a subsample for chemical analysis. Samples from 2001-02, 2014, and 2015 were measured for pH in 0.01 mol/L $CaCl_2$ (Robarge and Fernandez, 1987). All archived 2001-02 samples, and new 2014-15 samples were analyzed in 2016 for carbon and nitrogen on a CN elemental analyzer (CE-Elantech Thermo FlashEA 1112 Series NC Soil Analyzer) using pulverized subsamples. Soil standards obtained from the North American Proficiency Testing program were used to standardize the instrument. Exchangeable cations were also measured in 2016 on all samples from both time periods in an extract obtained from a mechanical vacuum extractor using 1 M NH_4OAc buffered at pH 4.8. Cation concentrations were measured with an Agilent inductively coupled plasma spectrometer (Agilent Technologies 700 Series ICP-OES) at the US Forest Service laboratory in Durham, NH. Reference samples of Oa and Bs horizons from Vermont

were included in all analytical streams and yielded values of C, N, pH, and exchangeable cations comparable to the median values reported in an interlaboratory study (Ross et al., 2015). All profile descriptions and chemistry data will be published on the US Forest Natural Resource Manager (U.S. Forest Service, NRM).

The 2001-02 exchangeable cation determinations (Al, Ca, Mg, Mn, Na, and K) were originally measured in 1 M NH_4Cl extracts obtained by mechanical vacuum extraction (Blume, 1990). 30 archived samples from 2001-02 were randomly selected and re-analyzed in 2017 using 1 M NH_4Cl to determine if changes had occurred due to archiving or method differences. The re-analysis was completed by the same laboratory that made the original measurements. Regression showed new analyses of the 2001-02 archived samples were highly correlated with original analyses. The Al, Ca, Mg, Mn, and K concentrations were less than 5% lower in recent measurements, though there was a high correlation (r^2 = 0.86 for Al; 0.95 for Ca; 0.87 for Mg; 0.97 for Mn, 0.94 for K). Na, however, had an intercept of 7.18 and a slope of 1.05 (r^2 = 0.10). The high correlation of Al, Ca, Mg, Mn, and K suggests change was not detectable and change is smaller than the detection limit in archived samples. The consistently higher concentrations of Na may have resulted from the differences in the extracts and analytical noise on the ICP.

4.2.3 Statistical analyses

Differences among observers may have led to sampling more than one subhorizon in the first sampling year compared to one horizon in another sampling year. Therefore, genetic horizons were combined into general categories for comparison of results between sample years. Oa, spodic, transition, and C horizon categories were created to include all samples separated into subhorizons (e.g. Oa1 and Oa2). A general spodic horizon category combined all illuvial B

horizons, including Bhs, Bh, and Bs and the transition horizon category included BC and CB horizons. Temporal change in E horizons was not explored because E horizons were typically thin and discontinuous, and their low organic matter content makes them uniformly low in C and N content and extractable cations.

Analytical results for individual genetic horizons were aggregated into a general horizon category by using a weighted average to determine overall exchangeable cations, pH, C and N concentration. The weighted average was calculated by multiplying the thickness, bulk density, and one minus the proportional coarse fragments to determine a unit area mass for every individual horizon within a general horizon. The individual horizon mass was then divided by the sum of all horizon masses in the general horizon, multiplied by a soil chemistry variable measured, and the sum of products used for the general horizon value. Bulk density was estimated by the relationship with organic matter reported by (Federer et al., 1993) and assuming organic matter is 50% carbon. Across all plots, average top and bottom depths (cm) and color were calculated by general horizon category for both sampling years. Munsell colors were averaged by converting colors to RGB color coordinates, averaged by general horizon category for the purposes of comparison, and then converted back to Munsell color to report averages by general horizon category using the 'aqp' package in R (Beaudette et al., 2013).

Pairwise t-tests of mean top and bottom depths, color, pH, C, N, and log-transformed cation concentrations were used to compare years on a plot by plot basis for the first objective of this study when the horizon was present during both sample times. For example, Oa horizons were present in 25 plots during both sampling years, whereas spodic horizons were present in both

sampling years in all 37 plots. In addition, a Wilcoxon signed-rank test was used to compare years on a plot by plot basis on non-transformed cation concentrations.

Pooled variance was calculated to determine within-plot spatial variability (eq 1). The pooled approach for calculating variance accounts for the lack of variance present from the first sampling time since variance cannot be calculated using one sample; at the second sampling time, the number of samples (5) is very small for obtaining a reliable estimate of the variance. A pooled variance loses site-specific information about the variability, but provides a more reliable estimate of the variability that would be encountered under typical conditions. The pooled variance is calculated as:

$$s^2 = \frac{1}{(\sum n_j) - n_i} \sum (x_{ij} - \bar{x_j})^2 \qquad \text{[eq 4.1]}$$

where x_{ij} is the *i*th pit of the *j*th site and $\bar{x_j}$ is the sample mean of the site. The total number of pits sampled from both samplings is n_j and n_i represents the total number of subsampled sites. The magnitude of change that could be accounted for based on sampling variability alone is then determined as the standard error of the difference between two sets of measurements, one based on a single pit and one based on multiple pits, with the sampling variance for a single pit estimated as the pooled variance, i.e.:

$$s_\Delta = \sqrt{s^2 + \frac{s^2}{n_{t2}}} \qquad \text{[eq 4.2]}$$

where s_Δ is the standard error of the estimated change, n_{t2} is the number of pits sampled from the second sampling time at the *j*th site. To evaluate the influence of variability on the sample size needed to detect plot-specific change, we used a power analysis approach. Required sample

sizes were calculated based on the pooled variances of the subset of 6 intensively sampled plots, with a power (i.e., probability of a statistically-significant change detection) of 0.8 and significance of 0.05 to detect plot-specific change and the observed magnitude of change found across all 37 plots.

For the second objective, plots were partitioned into three groups, vertical, lateral, or bimodal, representing the dominant hydrologic pathway influencing soil formation. Vertical hydrologic development was defined as profiles with morphology indicating a lack of watertable incursion in the solum (Gannon et al., 2014). Lateral sites had morphology indicating regular water saturation throughout the solum (Sommer, 2006) while bimodal sites were intermediate with some evidence of watertable influence primarily in the lower portion of the solum (Bailey et al., 2014). Figure 4.2 depicts representative soil profiles (plots GC2, GR3, and GC3) of vertical, lateral, and bimodal hydrologic regimes that influence soil horizon sequence.

Topography, horizon sequences, and soil profile characteristics were all used to assign each plot to a hydrologic group (Bailey et al., 2014). A multivariate analysis of variance (MANOVA) was used to evaluate temporal change between 2014 and 2001-02 in C, N, pH, and exchangeable cation concentrations between hydrologic groups. To assess the influence of this stratification on change detection, an ANOVA power analysis was also completed to determine how many sites of each hydrologic group were necessary for detecting a significant difference ($\alpha = 0.05$) with a power of 0.8. All analyses were completed using base packages in R (R Development Core Team).

Figure 4.2: Representative soil profiles (GC2, GR3, and GC3) from 2001-02 depicting the common horizon sequence associated with the dominant hydrologic pathway influencing a soil developed vertically, laterally, or bimodally. Plots were partitioned into three hydrologic groups based on topography, horizon sequences, and soil profile characteristics (Bailey et al., 2014). Laterally influenced profiles generally lacked an E horizon and a Bh horizon was the dominant illuvial horizon type. Bimodal profiles may have a thin E horizon and had a Bh horizon underneath a lighter colored Bhs and or Bs horizon. Brackets parallel to each soil profile indicate the subhorizons aggregated within spodic and transition categories for comparison.

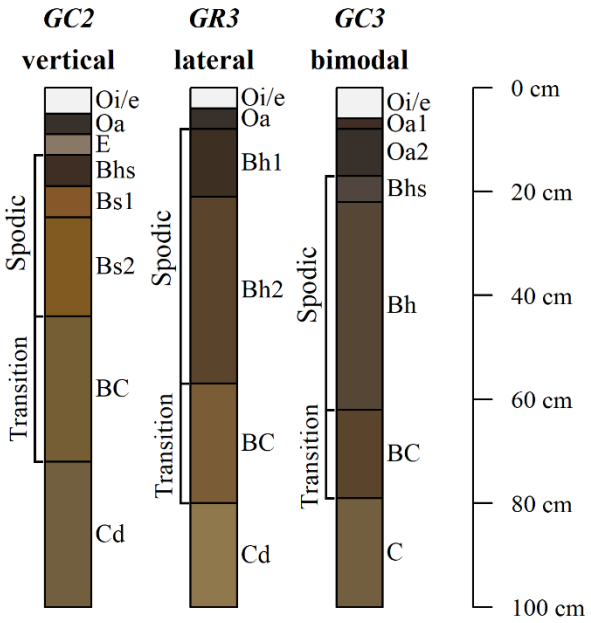

4.3 RESULTS

4.3.1 Overall decadal soil change

There were no significant differences in sampling depths or color by general horizon between sampling years except for a slightly greater bottom depth of sampling of the C horizon in the original 2001-02 sampling years (Table 4.1).

Table 4.1: Average top and bottom depths and color by sample year listed for each general horizon category (Oa, spodic, transition, and C). The number of plots with each general horizon category present in both sampling years indicated by n. The bottom depth of the C horizon is the depth observed, not necessarily the bottom of the horizon. Average colors were calculated by converting Munsell colors to RGB color coordinates, calculating the mean, and converting back to Munsell color.

General horizon	*n*	Year	Top (cm)	Bottom (cm)	Average Color
Oa	25	2001-02	3.9	9.9	10YR 2/1
		2014	3.6	9.2	7.5YR 2/1
Spodic	37	2001-02	13.4	48.2	7.5YR 3/3
		2014	14.9	54.6	7.5YR 3/3
Transition	32	2001-02	47.8	84.0	10YR 4/5
		2014	51.5	87.1	10YR 4/4
C	37	2001-02	80.2	115.7	2.5Y 5/3
		2014	82.7	102.1	2.5Y 4/3

Mean carbon (C) and nitrogen (N) concentration (g kg -1), pH, and exchangeable cation concentration ($cmol_c\ kg^{-1}$) for each general horizon category (Oa, spodic, transition, and C) by sampling year are listed in Table 4.2. Significant differences between sample years are in indicated in bold. The results from the paired t-tests found significant increases in C and N of the Oa horizons with approximately 30% higher C concentrations in 2014 than in 2001-02. A smaller but significant decrease in C concentration also occurred in the transition horizons.

Table 4.2: Average carbon (C) and nitrogen (N) concentration (g kg $^{-1}$), pH, and exchangeable cation concentration (cmol$_c$ kg^{-1}) for each general horizon category (Oa, spodic, transition, and C) by sampling year. Paired t-tests were performed to determine differences between sample years. Significance testing was conducted on log-transformed cation concentrations when residuals did not meet normality. Significant differences between sample years are indicated in bold.

General horizon	*n*	Year	C	N	pH	Al	Ca	K	Mg	Mn	Na
			g kg^{-1}			cmol$_c$ kg^{-1}					
Oa	25	2001-02	**33.4**	**1.6**	3.12	**5.00**	**9.69**	**0.75**	**1.77**	0.47	0.09
		2014	**42.6*****	**2.0*****	3.21	**3.47***	**13.61***	**1.07***	**2.27***	0.46	0.08
Spodic	37	2001-02	5.4	270	3.67	**13.21**	**0.45**	0.08	**0.09**	0.03	**0.03**
		2014	5.3	290	3.77	**17.89*****	**0.40****	0.07	**0.08****	0.02	**0.02*****
Transition	32	2001-02	**1.2**	70	4.14	**6.92**	**0.20**	0.04	0.03	0.01	0.02
		2014	**1.0****	60	4.22	**8.79****	**0.12****	0.03	0.02	0.00	0.02
C	37	2001-02	0.6	30	4.30	**3.22**	0.14	0.03	0.03	0.01	0.02
		2014	0.6	30	4.34	**6.67*****	0.21	0.03	0.07	0.01	0.02

*Significant at the 0.05 probability level.
**Significant at the 0.01 probability level.
***Significant at the 0.001 probability level.

There were no significant differences in pH at any depth, although the 37 soil profiles were consistent with chemical indicators of Spodosols by exhibiting increasing pH by depth (Table 4.2 and Supplemental Figure S4.1).

Paired t-tests on log-transformed cation concentrations found significant decreases in Al in Oa horizons and mean exchangeable Al was 1.5 times higher in 2001-02 than in 2014 within Oa horizons. Conversely, significant increases of Ca, K, and Mg occurred in the Oa horizon. Significant increases in Al occurred in spodic horizons and mean exchangeable Al was approximately 35% lower in 2001-02 than in 2014 within spodic horizons. Significant increases in Al below the Oa horizons were not coupled with any detectable change in pH (Supplemental Figure S4.1). Significant decreases in Ca, Mg, and Na concentrations were also detected in the spodic horizons. A significant increase of 27% in Al concentration was found in the transition horizons. Mean exchangeable Ca was approximately 1.6 times higher in 2001-02 then 2014 in the transition horizons. Finally, a significant increase in Al concentrations occurred in the C horizons. The non-parametric analyses yielded similar results and no difference in interpretation as the paired t-tests.

4.3.2 Within-site pooled variance

We found that within-site variability was comparable to overall regional variability across the WMNF. Table 4.3 provides the standard deviation of concentrations of carbon (C), and exchangeable cations (Al, Ca, K, Mg, Mn, and Na) from 1 soil pit at each of the thirty-seven plots sampled in 2014 (“All 2014”) as well as standard deviation calculated from the pooled variances from 5 soils pits at each of the 6 intensively sampled plots sampled in 2014-15 (“Subset 2014-15”).

Table 4. 3: Standard deviation of the concentrations of carbon (C), and exchangeable cations (Ca, K, Mg, Mn, and Na) from 1 soil pit at each of the thirty-seven plots sampled in 2014 ("All 2014"). Standard deviation calculated from the pooled variances of C, Ca, K, Mg, Mn, and Na from 5 soils pits at each of the 6 intensively sampled plots sampled in 2014-15 ("Subset 2014-15").

General horizon	Top†	Bottom†	C	Al	Ca	K	Mg	Mn	Na
			g kg^{-1}	———		$cmol_c$ kg^{-1}		———	
Oa (All 2014)	3.6	9.2	0.06	1.54	0.90	0.59	0.59	1.26	0.30
Oa (Subset 2014-15)	4.1	9.8	0.06	1.48	0.99	0.48	0.65	1.12	0.42
Spodic (All 2014)	14.9	54.6	0.03	0.39	1.20	0.67	0.93	0.97	0.45
Spodic (Subset 2014-15)	15.8	53.1	0.03	0.45	1.05	0.76	0.97	1.17	0.53
Transition (All 2014)	51.5	87.1	0.01	0.40	1.14	0.77	1.14	0.75	0.60
Transition (Subset 2014-15)	50.6	81.2	0.01	0.41	1.05	1.13	1.31	1.19	0.64

† Average top and bottom depths (cm).

Overall, exchangeable Al concentrations exhibited the highest variance both at the within-plot scale and landscape-scale across general horizons compared to the other analytes. Figure 4.3 depicts the exchangeable Al concentrations in each general horizon category from all 2001-02 and 2014 pits as well as from the 6 subset intensively sampled plots with one soil pit from 2001-02 compared to 5 soil pits sampled in 2014-15.

Figure 4.3: Extractable Al concentrations ($cmol_c\ kg^{-1}$) in each general horizon category from all 2001-02 ("All 2001-02) and 2014 ("All 2014") plots. In addition, Al from the 6 subset plots with one soil pit from 2001-02 ("Subset 2001-02") at each location and 5 soil pits sampled in 2014-15 at each location ("Subset 2014-15"). The Subset 2001-02 values represents 1 soil pit at each of the 6 sites and Subset 2014-15 values represent 5 total soil pits from each of the 6 sites. The box represents the 25th and 75th quantiles, the whiskers represent the 5th and 95th quantiles, the median is marked by a straight line, and outliers are indicated by a solid dot.

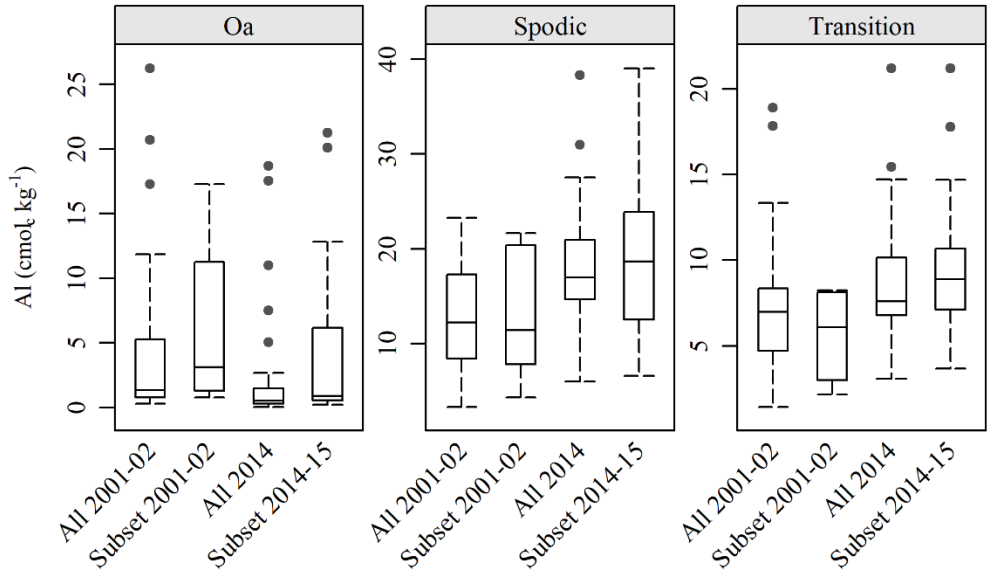

Higher variance in Al was found across all 2014 plots in the Oa horizon then in the pooled variance from the 6 subset of intensively sampled plots. Conversely, higher variance in Ca was found in the 6 subset plots intensively sampled in 2014-15 then all 2014 plots in the Oa horizon. Lower variance in Al was found across all 2014 plots in the spodic and transition horizons then in the pooled variance from the 6 subset plots intensively sampled in 2014-15. However, higher variance in Ca was found across all 2014 plots in the spodic and transition horizons then in the pooled variance from the 6 subset plots intensively sampled in 2014-15.

The number of plots needed to detect significant change ($\alpha = 0.05$) and equal magnitude of observed change for overall significant differences was calculated using a power analysis. For example, 7 within-plot soil pits were required from both sampling periods to detect the same magnitude of significant change in C of the Oa horizons as was found across all 37 plots. The power analysis also showed 20 within-plot soil pits were required from both sampling years to detect both significant change and the observed magnitude of overall change found from all plots of Al in the spodic horizons. The results from this pooled variance approach showed that at least 27 plot-specific samples from both sampling years across all horizons are necessary to detect significant change of the same magnitude as the overall change in Al observed at the WMNF scale. Similarly, at least 28 soil pits at one plot are needed from both sampling years across all horizons to detect significant temporal change in Ca. However, for analytes with higher variances, including K, Mg, and Mn, more pits at both a site-specific and landscape scale would be required in subsequent sampling years to detect change.

4.3.3 Stratification by hydrologic groups

The 2001-02 and 2014 element concentration differences between sampling years for the 3 dominant hydrologic groups influencing soil development, including vertical, lateral, or bimodal were calculated using MANOVA. There were 22 plots designated as developed vertically, 9 developed laterally, and 6 developed bimodally. The MANOVA results within the Oa horizon were significantly different ($p < 0.002$) between groups with an F-value of 3.290 (Pillai-Bartlett test statistic). Only 25 sites had an Oa present from both sampling years in 2001-02 and 2014; within those sites that had an Oa present, 18 of those sites were developed vertically, 4 were developed laterally, and 3 sites were identified as bimodal. Significant differences between groups in the Oa horizon were found in C (g kg^{-1}), Ca ($cmol_c$ kg^{-1}), and Na with F-values of 4.15, 2.70, and 15.6 respectively (Figure 4.4). There were no significant differences in the Oa horizon of N, pH, Al, K, Mg, and Mn (F-value < 2.00).

Figure 4.4: Significant differences between 2001-02 and 2014 for the Oa horizon in C (g kg^{-1}) and Ca, and Na concentrations ($cmol_c$ kg^{-1}) by hydrologic group. Groups represent the dominant hydrologic flowpaths influencing soil development, including vertical, lateral, or bimodal.

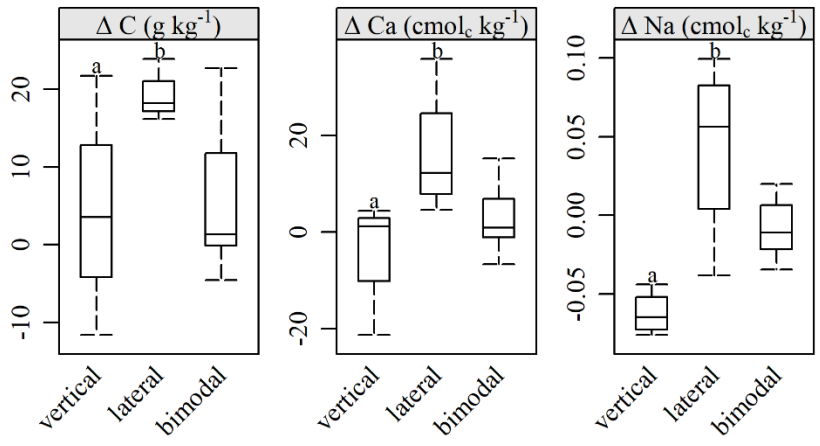

Oa horizons at sites that developed laterally showed significant increases in exchangeable Ca by 3.5 times from 2001-02 to 2014. Oa horizons at sites that developed vertically or bimodally showed a mean increase of approximately 1.3 times higher in 2014 than in 2001-02 or stayed approximately the same respectively. There were no significant differences of element concentrations in the other horizons (spodic, transition, and C) between hydrologic groups. Insignificant changes included increasing in Al and decreases in Ca in the spodic horizons at sites developed vertically, whereas Al in the spodic horizons decreased at sites developed laterally and Ca increased.

ANOVA power analysis was completed to determine how many sites per hydrologic group were necessary for significant ($\alpha = 0.05$) difference detection. For example, 14 was the smallest sample size per hydrologic group at the landscape-scale needed to detect significant change of C, Al, Ca, and Na in the Oa horizon. However, 20 was the smallest sample size per hydrologic group at the landscape-scale needed to detect a significant change of C, Al, Ca, and Na in the spodic and transition horizons. Sample sizes per dominant hydrologic group in the Oa horizon ranged from the 14-36, the fewest for Al, Ca, and Mg, and the most pH, Mn, and Na. Selecting the element with the largest sample size will enable detection of differences for the other elements.

4.4 DISCUSSION

4.4.1 Study design options for maximizing temporal change detection

Differences between observers resampling a site as well as spatial variation in soils are common obstacles in detecting temporal change in soil chemistry (Lawrence et al., 2013). For example, sampling the Oa horizon deeper into the mineral horizon one sampling year than another

sampling period can result in lower concentrations of C, as observed in 2001-02 from this study. In addition, differences in the presence and thickness of genetic horizons, caused by small scale spatial variation, can inhibit detection of soil change over time. Therefore, ensuring sampling consistency, particularly depth, as well as methods for comparing differing horizon sequences are essential for comparing measurements between time periods. Previous soil resampling studies have implemented various protocols to ensure consistency. For example, Bailey et al. (2005) used a combined Oa/A and the horizon sample straddling specific depths, e.g. the 50 cm and 100 cm depths for comparing two sampling periods. Bedison and Johnson (2010) pooled previous sampling measures into appropriate depth intervals based on the most recent sampling intervals. Our study also leveraged a pooled horizon approach by aggregating subhorizons into a general genetic horizon category. Any differences in horizon depths or colors that might have occurred between sampling years were not great enough to be detected with the study methods. Spatial variability in these measures can be much greater than expected from temporal changes over a decade, results suggested that sampling was done consistently to minimize those effects and that spatial variability was well addressed with these methods.

Another challenge in this study arose from the paired re-sampling design, which could not account for within-plot variability from one soil pit per site over two sampling time periods. It is often anticipated that magnitude of soil variability increases with the size of the study area. However, we found that within-site variability was comparable to overall regional variability across the WMNF. The pooled variance approach to estimate the magnitude of change necessary to detect plot-specific change equal to overall significant change loses site-specific information about within site variability, but provides a more reliable estimate of the change over time at the WMNF scale. Therefore, our study suggests the magnitude of change across the WMNF was

greater than potential differences between observers, sampling depth, and within-plot spatial variability. Confining the boundaries of this study based on physiographic characteristics was important for limiting spatial variability and likely more difficult to address beyond the White Mountain region.

4.4.2 Temporal change on the WMNF compared to other studies

Declines in acidic deposition across Europe and North America (Lehmann et al., 2005; Greaver et al., 2012) have led to signs of chemical recovery of soils from acidification (Lawrence et al., 2015; Berger et al., 2016). Lawrence et al. (2012) also reported significant Al decreases in the Oa horizon at two sites on the WMNF where red spruce was a major species in the canopy, and a significant Ca decrease in upper B horizon at one of the two sites. In addition, Lawrence et al. (2015) reported overall decreases of exchangeable Al in the O horizon as early indications of recovery while decreases in base saturation of mineral horizons continued at some sites. Changes in Al and Ca within the deeper parts of the profile (transition and C horizon) have not been previously reported since past research commonly focused on O and upper B horizons. The overall decrease in Al and increase in Ca within the Oa horizons across the WMNF are consistent with indications of recovery, but were coupled with continued acidification in the spodic and transition horizons as indicated by increases in exchangeable Al concentrations in deeper portions of the soil profile.

The results from this study indicate vertical mobilization of exchangeable Al from the upper forest floor into the rooting zone of trees which has long-term implications on forest health. Recovery from acid deposition in soil chemistry would be expected to result in decreases in Al and increases in Ca of the mineral horizons. Subsequent sampling periods, as this study

continues at an approximately decadal resampling scale into the future, may reveal a longer term temporal trajectory of increased Al and mobilization deeper into the soil profile and perhaps an eventual decrease as excess Al accumulated over the acid deposition period is flushed from the soil system. It is unlikely the observed decadal change is caused by natural soil development since podzolization occurs over a much larger time-scale. The significant results in the Oa horizon from soil resampling are more consistent with reports suggesting indications of recovery.

4.4.3 Hydrologic gradients for stratifying soil monitoring

Partitioning sample sites by the dominant hydrologic pathway influencing soil formation may help reduce landscape-scale soil chemistry heterogeneity and potentially increase sensitivity of change detection associated with specific horizons. Sites developed by vertical hydrologic flow were more susceptible to leaching processes as buffering from atmospheric deposition and mineral weathering is more limited. Sites developed by lateral hydrologic regimes were less susceptible to depletion processes and potentially more responsive to recovery processes from the influence of shallow groundwater and solute inputs from upslope. Significant differences by dominant hydrologic pathways in the Oa horizons suggests high turnover may contribute to faster rates of detectable change whereas the rates of detectable change in deeper portions of soil profiles may be slower. Hazlett et al. (2011) also discussed the effect of topographic position on detectable soil chemical changes and found increases in base cation concentrations in upper mineral soil horizons for plots in poorly drained convergent topographic locations.

In addition, our ability to identify the areal extent and topographic features commonly associated with different hydrologic influences on soil formation has greatly improved and was not considered when the sites in this study were originally established. However, the uneven number

of sites for this study within each hydrologic group could influence detection between groups in the spodic, transition, or C horizons. Most of the plots in this study were developed vertically which could contribute to the overall regional detection of significant Al change in the Oa horizons. Whereas the 9 plots developed laterally are contributing to the overall Al distribution within the spodic and transition horizons. An even number of sites within each hydrologic group could be selected in future studies by delineating the areal extent of the dominant hydrologic patterns influencing soil formation for initial design stratification. In regions where hydrologic gradients occur across the landscape, we recommend this method of stratification to help identify sites more susceptible to change. For example, in this study, the WMNF could continue resampling the 37 permanent plots, intensively sample the 6 subset plots, and consider intensively sampling more plots that were developed laterally or bimodally.

4.5 CONCLUSIONS

A rapidly changing environment has highlighted the need for more effective and site-specific soil monitoring over short time scales. This regional soil monitoring approach investigated a paired-resampling design by general genetic horizon groups to detect significant decadal change in soil chemistry within the same general soil and forest type. The monitoring design was created for the WMNF to establish a long-term understanding of how soil chemistry is changing at a landscape scale and to inform soil quality standards. The results from this study highlight how within-site variability is equal to the landscape-scale of Spodosols in northern hardwood forests. Finally, it is important to incorporate landscape-soil-water dynamics when characterizing change by the dominant processes of soil formation and horizonation because groundwater influenced

soils were more responsive to recovery processes in the Oa horizons compared to soils developed vertically via unsaturated flow.

From a forest management perspective, an ecosystem's response to changes in soil properties provides the context to determine how potential soil property changes may affect ecosystem composition, processes and function. This serves as the basis for national forests and other forest land managers to determine whether a response to a management activity is moving the ecosystem towards or away from a desired condition. This approach to estimate the variance components simultaneously at the landscape scale, and at the within-plot or micro-scale is crucial for calculating sample size and increases our technical understanding of how management or external forcings such as air pollution or climate change may alter soil over time.

CHAPTER 5
CONCLUSIONS

5.1 INTRODUCTION

Identifying the areal extent of bedrock outcrops and associated shallow soil has important implications in understanding the spatial dynamics of surrounding vegetation, stream chemistry gradients, and soil formation. Manual methods of delineating bedrock outcrops and shallow soil are still commonly employed in the northeastern US, expensive to employ over broad areas and limited by the geometry of polygon units. Therefore, it is crucial we improve the accuracy and efficacy in our approach to delineate bedrock outcrops and associated shallow soil in the northeastern US. Chapter 2 illustrated our ability to accurately interpret the presence of bedrock outcrops and shallow soil from high resolution lidar-derived shaded relief maps through visual estimates in order to achieve a statistically valid sample size. Additionally, we were able to improve the accuracy and efficiency in delineating the presence of bedrock outcrops and associated shallow soil in comparison to manual delineation methods using three topographic metrics at Hubbard Brook Experimental Forest as well as across a second validation watershed 16 km northwest.

Predicting the asymptotic range of stand relative density and biomass has important implications on silvicultural practices and understand forest carbon pools in late successional forests across northeastern US. Additionally, quantifying the influence of site quality on carrying capacity in a mixed species forest is a long-standing challenge and has not been thoroughly tested with long-

term longitudinal data. Chapter 3 concluded the stand-level variability of stand relative density appeared to be larger than previously assumed. The variability associated with the plot-level random effects suggested broad differences in structure among the plots could be accounted for with a topographic metric as a proxy for site quality and highlighted the importance of incorporating landscape-soil-water dynamics when characterizing stand dynamics and growth. The management implications of the stand-level variability suggested site quality may need to be considered when employing density management protocols.

Finally, a primary challenge for soil monitoring is to disentangle heterogeneity at multiple spatial scales so variation occurring over space is not confounded with change across time. Therefore, Chapter 4 objectives were to investigate overall change in soil chemistry of mid-elevation, northern hardwood Spodosols, calculate the variance components at multiple spatial scales, and stratify sampling sites by dominant hydrologic pathways to determine if groundwater influenced soils were more responsive to acidification recovery processes compared to soils developed vertically via unsaturated flow. Significant increases in carbon and base cations and a decrease in Al in the Oa horizon while base cations decreased and Al increased in some mineral horizons were found from forty permanent plots sampled across the WMNF in 2001-02 and resampled in 2014. Additionally, within-site variability was comparable to overall variability across the WMNF. When study sites were stratified into hydrologic groups, we found an even stronger signal of increasing carbon and base cation concentrations from 2001-02 to 2014 for the Oa horizon, suggesting that soils influenced by shallow groundwater contributions from upslope were more responsive to acidification recovery than soils influenced only by vertical percolation.

5.2 BROADER IMPLICATIONS

Although Chapter 2 explored the binary predictions of various classifiers, the results suggested a multinomial classification, including other HPU types, may be possible. Since HPU mapping requires delineation of bedrock outcrops and associated shallow soil (Gillin et al., 2015a), the framework presented in Chapter 2 greatly improves the accuracy, efficiency, and geographic extent of applying HPU models beyond HBEF. In addition, the HBEF database is well suited for creating a valley wide HPU model covering the full range of HPUs, not just limited to four soil classifications as previously explored. The WAMMO soil database also serves as an independent source for future HPU model validation. Finally, the predictive modeling in Chapter 2 can also serve NRCS in their efforts to create digital soil maps across Vermont and New Hampshire since they are required to delineate bedrock outcrops and associated shallow soils.

The results from Chapter 3 warrant further investigation in the influence of site quality on both stand relative density and biomass. This study likely represents the first successful effort to quantify these relationships using variables that are widely available at a landscape scale. Chapter 3 methods, however, only explored the influence of reducing stand-level variability using one topographic metric as a covariate. Preliminary investigations suggest that more than one topographic covariate may reduce variability and an additional covariate applied to the second random effect may also improve model results. Additionally, an attempt to compile and gather more information regarding soil properties at a randomly selected subset of unmanipulated plots would assist in confirming whether the specific topographic metrics used in Chapter 3 are appropriate proxies of site quality at BEF. For example, topographic wetness index (TWId) (Beven and Kirkby, 1979) was computed with the upslope accumulated area (UAA)

using multiple triangular flow direction algorithm (Seibert and McGlynn, 2007) as the numerator and a 5 m analysis window for downslope index (Hjerdt et al., 2004) as the denominator. Previous studies at HBEF concluded that TWId, although multiple TWI variants were explored, was strongly correlated with soils influenced by lateral hydrologic regimes and largely explained the transition between typical and bimodal podzols to Bh podzols (Bailey et al., 2014). The automation of bedrock outcrops and associated shallow soil delineation from Chapter 2 also has important implications for exploring the full extent of HPUs on stand relative density and biomass at BEF. Finally, we could gain a better understanding of stand growth between 30 and 50 years of stand age if BEF manipulated stand data are incorporated. The inclusion of manipulated stand data may contradict the Chapter 3 conclusions that a Chapman-Richards growth function was a better fit than a logistic function.

Chapter 4 introduced a new approach in comparing soil colors by observer with paired t-tests. Further investigations are warranted in better understanding and quantifying the differences among observers. Quantifying differences observers could contribute to understanding the influence of sampling by depth rather than by genetic horizons. Additionally, Chapter 4 reported the overall change detection across the WMNF as consistent with previous studies and was the first study to report within-plot variability was equal to variability across the WMNF. These results will directly inform soil monitoring programs in calculating sample size. As the WMNF continues monitoring the forty permanent plots, it will be important to continue intensively sampling a subset of the plots to ensure these variance components are the same in subsequent inventory years. Finally, Chapter 4 also introduces a new concept that rates of temporal change may not occur equally in soils developed from vertical rather than lateral hydrologic regimes influencing soil formation. Although the results were significant for the Oa horizon (4-10 cm),

subsequent sampling years may reveal significant differences in the spodic and transition horizons.

LIST OF REFERENCES

Akaike, H. 1974. A new look at the statistical model identification. IEEE Trans. Autom. Control 19(6): 716–723.

Arp, H., and C. Tranarg. 1982. Mapping in tropical forests: a new approach using the laser APR [Airborne Profile Recorder]. Photogramm. Eng. Remote Sens. http://agris.fao.org/agris-search/search.do?recordID=US19830884206 (accessed 14 February 2018).

Ashraf, M.I., Z. Zhao, C.P.-A. Bourque, and F.-R. Meng. 2012. GIS-evaluation of two slope-calculation methods regarding their suitability in slope analysis using high-precision LiDAR digital elevation models. Hydrol. Process. 26(8): 1119–1133. doi: 10.1002/hyp.8195.

Bailey, S.W. in review. Soil profile data for the Hubbard Brook Experimental Forest. www.hubbardbrook.org.

Bailey, S.W., P.A. Brousseau, K.J. McGuire, and D.S. Ross. 2014. Influence of landscape position and transient water table on soil development and carbon distribution in a steep, headwater catchment. Geoderma 226: 279–289.

Bailey, S.W., J.W. Hornbeck, and J.W. Hornbeck. 1992. Lithologic composition and rock weathering potential of forested, glacial-till soils. Res Pap NE-662 Radn. PA US Dep. Agric. For. Serv. Northeast. For. Exp. Stn. 7 P 662. doi: 10.2737/NE-RP-662.

Bailey, S.W., S.B. Horsley, and R.P. Long. 2005. Thirty years of change in forest soils of the Allegheny Plateau, Pennsylvania. Soil Sci. Soc. Am. J. 69(3): 681–690.

Bailey, S.W., K.J. McGuire, D.S. Ross, M.B. Green, and O.L. Fraser. in review. Mineral weathering and podzolization control acid neutralization and streamwater chemistry gradients in upland glaciated catchments, northeastern USA. Submitt. Front. Earth Sci.

Bal, T.L., A.J. Storer, M.F. Jurgensen, P.V. Doskey, and M.C. Amacher. 2015. Nutrient stress predisposes and contributes to sugar maple dieback across its northern range: a review. For. Int. J. For. Res. 88(1): 64–83. doi: 10.1093/forestry/cpu051.

Barrett, L.R., and R.J. Schaetzl. 1998. Regressive pedogenesis following a century of deforestation: evidence for depodzolization. Soil Sci. 163(6): 482.

Beaudette, D.E., P. Roudier, and A.T. O'Geen. 2013. Algorithms for quantitative pedology: A toolkit for soil scientists. Comput. Geosci. 52: 258–268. doi: 10.1016/j.cageo.2012.10.020.

Bedison, J.E., and A.H. Johnson. 2010. Seventy-Four Years of Calcium Loss from Forest Soils of the Adirondack Mountains, New York. Soil Sci. Soc. Am. J. 74(6): 2187–2195. doi: 10.2136/sssaj2009.0367.

Belcher, C.F. 1980. Logging railroads of the White Mountain. Appalachian Mountain Club, Boston, MA.

Belt, K., and S.T. Paxton. 2005. GIS as an aid to visualizing and mapping geology and rock properties in regions of subtle topography. GSA Bull. 117(1–2): 149–160. doi: 10.1130/B25463.1.

Berger, T.W., S. Türtscher, P. Berger, and L. Lindebner. 2016. A slight recovery of soils from Acid Rain over the last three decades is not reflected in the macro nutrition of beech (Fagus sylvatica) at 97 forest stands of the Vienna Woods. Environ. Pollut. 216: 624–635. doi: 10.1016/j.envpol.2016.06.024.

Beven, K.J., and M.J. Kirkby. 1979. A physically based, variable contributing area model of basin hydrology / Un modèle à base physique de zone d'appel variable de l'hydrologie du bassin versant. Hydrol. Sci. Bull. 24(1): 43–69. doi: 10.1080/02626667909491834.

Blume, L.J. 1990. Handbook of Methods for Acid Deposition Studies: Laboratory Analyses for Soil Chemistry. USEPA, Environmental Monitoring Systems Laboratory, Las Vegas, NV.

Bontemps, J.-D., and O. Bouriaud. 2014. Predictive approaches to forest site productivity: recent trends, challenges and future perspectives. For. Int. J. For. Res. 87(1): 109–128. doi: 10.1093/forestry/cpt034.

Bourgault, R.R., D.S. Ross, and S.W. Bailey. 2015. Chemical and Morphological Distinctions between Vertical and Lateral Podzolization at Hubbard Brook. Soil Sci. Soc. Am. J. 79(2): 428–439. doi: 10.2136/sssaj2014.05.0190.

Bourgault, R.R., D.S. Ross, S.W. Bailey, T.D. Bullen, K.J. McGuire, et al. 2017. Redistribution of soil metals and organic carbon via lateral flowpaths at the catchment scale in a glaciated upland setting. Geoderma 307: 238–252. doi: 10.1016/j.geoderma.2017.05.039.

Bravo-Oviedo, A., S. Condés, M. del Río, H. Pretzsch, and M.J. Ducey. 2018. Maximum stand density strongly depends on species-specific wood stability, shade and drought tolerance. For. Int. J. For. Res. 91(4): 459–469. doi: 10.1093/forestry/cpy006.

Breiman, L. 2001. Random Forests. Mach. Learn. 45(1): 5–32. doi: 10.1023/A:1010933404324.

Brus, D.J., B. Kempen, and G.B.M. Heuvelink. 2011. Sampling for validation of digital soil maps. Eur. J. Soil Sci. 62(3): 394–407. doi: 10.1111/j.1365-2389.2011.01364.x.

Buol, S.W., R.J. Southard, R.C. Graham, and P.A. McDaniel. 2011. Soil Genesis and Classification. John Wiley & Sons, Inc.

Burkhart, H.E., and M. Tomé. 2012. Modeling Forest Trees and Stands. Springer Science & Business Media.

Burton, W.C., G.J. Walsh, and Armstrong, Thomas R. 2000. Bedrock geologic map of the Hubbard Brook Experimental Forest, Grafton County, New Hampshire: U.S. U.S. Geological Survey, Reston, Virginia.

Chapman, D.G. 1961. Statistical problems in dynamics of exploited fisheries population. Proc. 4th Berkeley Symp. Math. Stat. Probab. 4(Berkeley: University of California Press.): 153–168.

Chojnacky, D.C., L.S. Heath, and J.C. Jenkins. 2014. Updated generalized biomass equations for North American tree species. For. Int. J. For. Res. 87(1): 129–151. doi: 10.1093/forestry/cpt053.

Clarholm, M., and U. Skyllberg. 2013. Translocation of metals by trees and fungi regulates pH, soil organic matter turnover and nitrogen availability in acidic forest soils. Soil Biol. Biochem. 63: 142–153.

Cogbill, C.V., J. Burk, and G. Motzkin. 2002. The forests of presettlement New England, USA: spatial and compositional patterns based on town proprietor surveys. J. Biogeogr. 29(10–11): 1279–1304. doi: 10.1046/j.1365-2699.2002.00757.x.

Cohen, J. 1960. A Coefficient of Agreement for Nominal Scales. Educ. Psychol. Meas. 20(1): 37–46. doi: 10.1177/001316446002000104.

Conant, R.T., G.R. Smith, and K. Paustian. 2003. Spatial Variability of Soil Carbon in Forested and Cultivated Sites. J. Environ. Qual. 32(1): 278–286. doi: 10.2134/jeq2003.2780.

Condés, S., P. Vallet, K. Bielak, A. Bravo-Oviedo, L. Coll, et al. 2017. Climate influences on the maximum size-density relationship in Scots pine (Pinus sylvestris L.) and European beech (Fagus sylvatica L.) stands. For. Ecol. Manag. 385: 295–307. doi: 10.1016/j.foreco.2016.10.059.

Congalton, R.G. 1991. A review of assessing the accuracy of classifications of remotely sensed data. Remote Sens. Environ. 37(1): 35–46. doi: 10.1016/0034-4257(91)90048-B.

Congalton, R.G., and L. Plourde. 2002. Quality assurance and accuracy assessment of information derived from remotely sensed data. Manual of Geospatial Science and Technology. Taylor & Francis, London. p. 349–361

Conrad, O., B. Bechtel, M. Bock, H. Dietrich, E. Fischer, et al. 2015. System for Automated Geoscientific Analyses (SAGA) v. 2.1.4. Geosci. Model Dev. 8(7): 1991–2007. doi: https://doi.org/10.5194/gmd-8-1991-2015.

Cronan, C.S., and D.F. Grigal. 1995. Use of Calcium/Aluminum Ratios as Indicators of Stress in Forest Ecosystems. J. Environ. Qual. 24(2): 209–226. doi: 10.2134/jeq1995.00472425002400020002x.

De Coninck, F. 1980. Major mechanisms in formation of spodic horizons. Geoderma 24(2): 101–128. doi: 10.1016/0016-7061(80)90038-5.

DeHayes, D.H., P.G. Schaberg, G.J. Hawley, and G.R. Strimbeck. 1999. Acid Rain Impacts on Calcium Nutrition and Forest HealthAlteration of membrane-associated calcium leads to membrane destabilization and foliar injury in red spruce. BioScience 49(10): 789–800. doi: 10.2307/1313570.

DiBiase, R.A., A.M. Heimsath, and K.X. Whipple. 2012. Hillslope response to tectonic forcing in threshold landscapes. Earth Surf. Process. Landf. 37(8): 855–865. doi: 10.1002/esp.3205.

Dormann, C.F., J. Elith, S. Bacher, C. Buchmann, G. Carl, et al. 2012. Collinearity: a review of methods to deal with it and a simulation study evaluating their performance. Ecography 36(1): 27–46. doi: 10.1111/j.1600-0587.2012.07348.x.

Drăguţ, L., and C. Eisank. 2011. Object representations at multiple scales from digital elevation models. Geomorphology 129(3): 183–189. doi: 10.1016/j.geomorph.2011.03.003.

Driscoll, C.T., G.B. Lawrence, A.J. Bulger, T.J. Butler, C.S. Cronan, et al. 2001. Acidic Deposition in the Northeastern United States: Sources and Inputs, Ecosystem Effects, and Management StrategiesThe effects of acidic deposition in the northeastern United States include the acidification of soil and water, which stresses terrestrial and aquatic biota. BioScience 51(3): 180–198. doi: 10.1641/0006-3568(2001)051[0180:ADITNU]2.0.CO;2.

Ducey, M.J., and R.A. Knapp. 2010. A stand density index for complex mixed species forests in the northeastern United States. For. Ecol. Manag. 260(9): 1613–1622. doi: 10.1016/j.foreco.2010.08.014.

Ducey, M.J., C.W. Woodall, and A. Bravo-Oviedo. 2017. Climate and species functional traits influence maximum live tree stocking in the Lake States, USA. For. Ecol. Manag. 386: 51–61. doi: 10.1016/j.foreco.2016.12.007.

FAO. 2003. Digital soil map of the world and derived soil properties. Food Agric. Organ. U. N. Land and Water Digital Media (version 3.5): http://www.fao.org/soils-portal/soil-survey/soil-maps-and-databases/.

Federer, C.A., J.W. Hornbeck, L.M. Tritton, C.W. Martin, R.S. Pierce, et al. 1989. Long-term depletion of calcium and other nutrients in eastern US forests. Environ. Manage. 13(5): 593–601. doi: 10.1007/BF01874965.

Federer, C.A., D.E. Turcotte, and C.T. Smith. 1993. The organic fraction–bulk density relationship and the expression of nutrient content in forest soils. Can. J. For. Res. 23(6): 1026–1032. doi: 10.1139/x93-131.

Galloway, J.N. 1995. Acid deposition: Perspectives in time and space. Water. Air. Soil Pollut. 85(1): 15–24. doi: 10.1007/BF00483685.

Gannon, J.P., S.W. Bailey, and K.J. McGuire. 2014. Organizing groundwater regimes and response thresholds by soils: A framework for understanding runoff generation in a headwater catchment. Water Resour. Res. 50(11): 8403–8419. doi: 10.1002/2014WR015498.

Gillin, C.P., S.W. Bailey, K.J. McGuire, and J.P. Gannon. 2015a. Mapping of Hydropedologic Spatial Patterns in a Steep Headwater Catchment. Soil Sci. Soc. Am. J. 79(2): 440–453. doi: 10.2136/sssaj2014.05.0189.

Gillin, C.P., S.W. Bailey, K.J. McGuire, and S.P. Prisley. 2015b. Evaluation of Lidar-derived DEMs through Terrain Analysis and Field Comparison. doi: info:doi/10.14358/PERS.81.5.387.

GRANIT. New Hampshire's Statewide Geographic Information System (GIS) Clearinghouse. NH GRANIT. http://www.granit.unh.edu/ (accessed 15 January 2018).

Greaver, T.L., T.J. Sullivan, J.D. Herrick, M.C. Barber, J.S. Baron, et al. 2012. Ecological effects of nitrogen and sulfur air pollution in the US: what do we know? Front. Ecol. Environ. 10(7): 365–372. doi: 10.1890/110049.

Grebby, S., J. Naden, D. Cunningham, and K. Tansey. 2011. Integrating airborne multispectral imagery and airborne LiDAR data for enhanced lithological mapping in vegetated terrain. Remote Sens. Environ. 115(1): 214–226. doi: 10.1016/j.rse.2010.08.019.

Gregoire, T.G. 1987. Generalized Error Structure for Forestry Yield Models. For. Sci. 33(2): 423–444. doi: 10.1093/forestscience/33.2.423.

Gruba, P., and J. Mulder. 2015. Tree species affect cation exchange capacity (CEC) and cation binding properties of organic matter in acid forest soils. Sci. Total Environ. 511: 655–662. doi: 10.1016/j.scitotenv.2015.01.013.

Guisan, A., S.B. Weiss, and A.D. Weiss. 1999. GLM versus CCA spatial modeling of plant species distribution. Plant Ecol. 143(1): 107–122. doi: 10.1023/A:1009841519580.

Gunn, J.S., M.J. Ducey, and A.A. Whitman. 2014. Late-successional and old-growth forest carbon temporal dynamics in the Northern Forest (Northeastern USA). For. Ecol. Manag. 312: 40–46. doi: 10.1016/j.foreco.2013.10.023.

Guo, Q., W. Li, H. Yu, and O. Alvarez. 2010. Effects of Topographic Variability and Lidar Sampling Density on Several DEM Interpolation Methods. Photogramm. Eng. Remote Sens. 76(6): 701–712. doi: 10.14358/PERS.76.6.701.

Hastie, T.J., R.J. Tibrhirani, and J. Friedman. 2009. The Elements of Statistical Learning: DataMining, Inference, and Prediction. 2nd ed. Springer, New York, NY.

Hastie, T.J., and R.J. Tibshirani. 1990. Generalized Additive Models. Monographs on Statistics and Applied Probability. Chapman and Hall, Hall

Haugerud, R.A., D.J. Harding, S.Y. Johnson, J.L. Harless, C.S. Weaver, et al. 2003. High-Resolution Lidar Topography of the Puget Lowland, Washington —A Bonanza for Earth

Science. GSA Today 13(6): 4. doi: 10.1130/1052-5173(2003)13<0004:HLTOTP>2.0.CO;2.

Hazlett, P.W., J.M. Curry, and T.P. Weldon. 2011. Assessing Decadal Change in Mineral Soil Cation Chemistry at the Turkey Lakes Watershed. Soil Sci. Soc. Am. J. 75(1): 287–305. doi: 10.2136/sssaj2010.0090.

Hengl, T., D.G. Rossiter, and A. Stein. 2003. Soil sampling strategies for spatial prediction by correlation with auxiliary maps. Soil Res. 41(8): 1403–1422. doi: 10.1071/sr03005.

Heung, B., H.C. Ho, J. Zhang, A. Knudby, C.E. Bulmer, et al. 2016. An overview and comparison of machine-learning techniques for classification purposes in digital soil mapping. Geoderma 265: 62–77. doi: 10.1016/j.geoderma.2015.11.014.

Hjerdt, K.N., J.J. McDonnell, J. Seibert, and A. Rodhe. 2004. A new topographic index to quantify downslope controls on local drainage. Water Resour. Res. 40(5): W05602. doi: 10.1029/2004WR003130.

Hoover, C.M., W.B. Leak, and B.G. Keel. 2012. Benchmark carbon stocks from old-growth forests in northern New England, USA. For. Ecol. Manag. 266: 108–114. doi: 10.1016/j.foreco.2011.11.010.

Hunckler, R.V., and R.J. Schaetzl. 1997. Spodosol Development as Affected by Geomorphic Aspect, Baraga County, Michigan. Soil Sci. Soc. Am. J. 61(4): 1105–1115. doi: 10.2136/sssaj1997.03615995006100040017x.

Hunter, I.R., and A.R. Gibson. 1984. Predicting Pinus radiata site index from environmental variables. N. Z. J. For. Sci. 14(1): 53–64.

Jenkins, J.C., D.C. Chojnacky, L.S. Heath, and R.A. Birdsey. 2003. National-Scale Biomass Estimators for United States Tree Species. For. Sci. 49(1): 12–35. doi: 10.1093/forestscience/49.1.12.

Jenny, H. 1941. Factors of Soil Formation: A System of Quantitative Pedology. McGraw-Hill, New York.

Johnson, C.E., A.H. Johnson, and T.G. Huntington. 1990. Sample size requirements for the determination of changes in soil nutrient pools. Soil Sci. 150(3): 637.

Keeton, W.S., A.A. Whitman, G.C. McGee, and C.L. Goodale. 2011. Late-Successional Biomass Development in Northern Hardwood-Conifer Forests of the Northeastern United States. For. Sci. 57(6): 489–505. doi: 10.1093/forestscience/57.6.489.

Keith, H., B.G. Mackey, and D.B. Lindenmayer. 2009. Re-evaluation of forest biomass carbon stocks and lessons from the world's most carbon-dense forests. Proc. Natl. Acad. Sci.: pnas.0901970106. doi: 10.1073/pnas.0901970106.

Kleinbaum, D., L. Kupper, A. Nizam, and K. Muller. 2013. Applied regression analysis and other multivariable methods. 5th ed. Cengage Learning, Boston, MA.

Kuhn, M. 2008. Building predictive models in R using the caret package. J. Stat. Softw. 28: 1–26.

Lawrence, G.B., I.J. Fernandez, D.D. Richter, D.S. Ross, P.W. Hazlett, et al. 2013. Measuring Environmental Change in Forest Ecosystems by Repeated Soil Sampling: A North American Perspective. J. Environ. Qual. 42(3): 623–639. doi: 10.2134/jeq2012.0378.

Lawrence, G.B., P.W. Hazlett, I.J. Fernandez, R. Ouimet, S.W. Bailey, et al. 2015. Declining Acidic Deposition Begins Reversal of Forest-Soil Acidification in the Northeastern U.S. and Eastern Canada. Environ. Sci. Technol. 49(22): 13103–13111. doi: 10.1021/acs.est.5b02904.

Lawrence, G.B., W.C. Shortle, M.B. David, K.T. Smith, R.A.F. Warby, et al. 2012. Early Indications of Soil Recovery from Acidic Deposition in U.S. Red Spruce Forests. Soil Sci. Soc. Am. J. 76(4): 1407–1417. doi: 10.2136/sssaj2011.0415.

Leak, W.B. 1982. Habitat mapping and interpretation in New England. Res Pap NE-496 Broomall PA US Dep. Agric. For. Serv. Northeast. For. Exp. Stn. 28p 496. https://www.fs.usda.gov/treesearch/pubs/15049 (accessed 18 May 2018).

Leak, W.B. 2006. Fifty-Year Impacts of the Beech Bark Disease in the Bartlett Experimental Forest, New Hampshire. North. J. Appl. For. 23(2): 141–143. doi: 10.1093/njaf/23.2.141.

Leak, W.B., and M.-L. Smith. 1996. Sixty years of management and natural disturbance in a New England forested landscape. For. Ecol. Manag. 81(1): 63–73. doi: 10.1016/0378-1127(95)03662-8.

Lefsky, M.A., W.B. Cohen, G.G. Parker, and D.J. Harding. 2002. Lidar Remote Sensing for Ecosystem StudiesLidar, an emerging remote sensing technology that directly measures

the three-dimensional distribution of plant canopies, can accurately estimate vegetation structural attributes and should be of particular interest to forest, landscape, and global ecologists. BioScience 52(1): 19–30. doi: 10.1641/0006-3568(2002)052[0019:LRSFES]2.0.CO;2.

Lehmann, C.M.B., V.C. Bowersox, and S.M. Larson. 2005. Spatial and temporal trends of precipitation chemistry in the United States, 1985–2002. Environ. Pollut. 135(3): 347–361. doi: 10.1016/j.envpol.2004.11.016.

Likens, G.E. 2013. Biogeochemistry of a Forested Ecosystem. Springer Science & Business Media.

Likens, G.E., C.T. Driscoll, and D.C. Buso. 1996. Long-Term Effects of Acid Rain: Response and Recovery of a Forest Ecosystem. Science 272(5259): 244–246. doi: 10.1126/science.272.5259.244.

Lim, K., P. Treitz, M. Wulder, B. St-Onge, and M. Flood. 2003. LiDAR remote sensing of forest structure. Prog. Phys. Geogr. Earth Environ. 27(1): 88–106. doi: 10.1191/0309133303pp360ra.

Lin, H., J. Bouma, L.P. Wilding, J.L. Richardson, M. Kutilek, et al. 2005. Advances in hydropedology. Adv. Agron. 85(10.1016/S0065-2113(04)85001–6): 1–89. doi: 10.1016/S0065-2113(04)85001-6.

Long, J.N. 1985. A Practical Approach to Density Management. For. Chron. 61(1): 23–27. doi: 10.5558/tfc61023-1.

Long, J.N. 1996. Technical Notes: A Technique for the Control of Stocking in Two-Storied Stands. West. J. Appl. For. 11(2): 59–61. doi: 10.1093/wjaf/11.2.59.

Long, R.P., S.B. Horsley, R.A. Hallett, and S.W. Bailey. 2009. Sugar maple growth in relation to nutrition and stress in the northeastern United States. Ecol. Appl. 19(6): 1454–1466. doi: 10.1890/08-1535.1.

Lundström, U.S., N. van Breemen, and D. Bain. 2000. The podzolization process. A review. Geoderma 94(2): 91–107. doi: 10.1016/S0016-7061(99)00036-1.

Luyssaert, S., E.-D. Schulze, A. Börner, A. Knohl, D. Hessenmöller, et al. 2008. Old-growth forests as global carbon sinks. Nature 455(7210): 213–215. doi: 10.1038/nature07276.

MacMillan, R.A., W.W. Pettapiece, S.C. Nolan, and T.W. Goddard. 2000. A generic procedure for automatically segmenting landforms into landform elements using DEMs, heuristic rules and fuzzy logic. Fuzzy Sets Syst. 113(1): 81–109. doi: 10.1016/S0165-0114(99)00014-7.

Mäkipää, R., M. Häkkinen, P. Muukkonen, and M. Peltoniemi. 2008. The costs of monitoring changes in forest soil carbon stocks. Boreal Environ. Res. 13: 11.

Mangold, R. 2000. Overview of the forest health monitoring program. Hansen Mark Burk Tom Eds Integr. Tools Nat. Resour. Invent. 21st Century Gen Tech Rep NC-212 St Paul MN US Dept Agric. For. Serv. North Cent. For. Exp. Stn. 129-140 212. https://www.fs.usda.gov/treesearch/pubs/15807 (accessed 5 August 2018).

McBratney, A.B., M.L. Mendonça Santos, and B. Minasny. 2003. On digital soil mapping. Geoderma 117(1): 3–52. doi: 10.1016/S0016-7061(03)00223-4.

McKenney, D.W., and J.H. Pedlar. 2003. Spatial models of site index based on climate and soil properties for two boreal tree species in Ontario, Canada. For. Ecol. Manag. 175(1): 497–507. doi: 10.1016/S0378-1127(02)00186-X.

McNab, W.H., and P.E. Avers. 1994. Ecological subregions of the United States: Section descriptions. Admin Publ WO-WSA-5 USFS Wash. DC.

Means, J.E., S.A. Acker, D.J. Harding, J.B. Blair, M.A. Lefsky, et al. 1999. Use of Large-Footprint Scanning Airborne Lidar To Estimate Forest Stand Characteristics in the Western Cascades of Oregon. Remote Sens. Environ. 67(3): 298–308. doi: 10.1016/S0034-4257(98)00091-1.

Miller, B.A., S. Koszinski, M. Wehrhan, and M. Sommer. 2015. Impact of multi-scale predictor selection for modeling soil properties. Geoderma 239–240: 97–106. doi: 10.1016/j.geoderma.2014.09.018.

Milodowski, D.T., S.M. Mudd, and E.T.A. Mitchard. 2015. Topographic roughness as a signature of the emergence of bedrock in eroding landscapes. Earth Surf. Dyn. 3(4): 483–499. doi: 10.5194/esurf-3-483-2015.

Muukkonen, P., M. Häkkinen, and R. Mäkipää. 2009. Spatial variation in soil carbon in the organic layer of managed boreal forest soil—implications for sampling design. Environ. Monit. Assess. 158(1–4): 67–76. doi: 10.1007/s10661-008-0565-2.

Næsset, E. 1997. Determination of mean tree height of forest stands using airborne laser scanner data. ISPRS J. Photogramm. Remote Sens. 52(2): 49–56. doi: 10.1016/S0924-2716(97)83000-6.

Nauman, T.W., J.A. Thompson, S.J. Teets, T.A. Dilliplane, J.W. Bell, et al. 2015. Ghosts of the forest: Mapping pedomemory to guide forest restoration. Geoderma 247–248: 51–64. doi: 10.1016/j.geoderma.2015.02.002.

Neary, D.G., C.C. Trettin, and D. Page-Dumroese. 2010. Soil quality monitoring: Examples of existing protocols. Page-Dumroese Deborah Neary Daniel Trettin Carl Tech Eds Sci. Backgr. Soil Monit. Natl. For. Rangel. Workshop Proc. April 29-30 2008 Denver CO Proc RMRS-P-59 Fort Collins CO US Dep. Agric. For. Serv. Rocky Mt. Res. Stn. P 61-82 59: 61–82.

Nezat, C.A., J.D. Blum, A. Klaue, C.E. Johnson, and T.G. Siccama. 2004. Influence of landscape position and vegetation on long-term weathering rates at the Hubbard Brook Experimental Forest, New Hampshire, USA1 1Associate editor: K. L. Nagy. Geochim. Cosmochim. Acta 68(14): 3065–3078. doi: 10.1016/j.gca.2004.01.021.

Nezat, C.A., J.D. Blum, R.D. Yanai, and B.B. Park. 2008. Mineral Sources of Calcium and Phosphorus in Soils of the Northeastern United States. Soil Sci. Soc. Am. J. 72(6): 1786–1794. doi: 10.2136/sssaj2007.0344.

NFMA. 1976. National Forest Management Act of 1976. 16 U. S. C. §§ 1600-1687. NFMA. https://www.fs.fed.us/emc/nfma/includes/NFMA1976.pdf (accessed 20 May 2018).

Oliver, C.D., and B.C. Larson. 1996. Forest stand dynamics: updated edition. John Wiley and sons.

Pearl, R., and L.J. Reed. 1920. On the Rate of Growth of the Population of the United States since 1790 and Its Mathematical Representation. Proc. Natl. Acad. Sci. 6(6): 275–288. doi: 10.1073/pnas.6.6.275.

Pinheiro, J., and D. Bates. 2000. Mixed-effects models in S and S-Plus. Springer, New York.

Pretzsch, H. 2009. Forest Dynamics, Growth and Yield: From Measurement to Model. Springer Science & Business Media.

Pretzsch, H., and P. Biber. 2005. A Re-Evaluation of Reineke's Rule and Stand Density Index. For. Sci. 51(4): 304–320.

Pretzsch, H., and P. Biber. 2016. Tree species mixing can increase maximum stand density. Can. J. For. Res. 46(10): 1179–1193. doi: 10.1139/cjfr-2015-0413.

R Development Core Team. R: A language and environment for statistical computing. R Found. Stat. Comput. Version 3.5.1.

Reineke, L.H. 1933. Perfecting a stand-density index for even-aged forests.

Rice, K.C., and J.S. Herman. 2012. Acidification of Earth: An assessment across mechanisms and scales. Appl. Geochem. 27(1): 1–14. doi: 10.1016/j.apgeochem.2011.09.001.

Richards, F.J. 1959. A Flexible Growth Function for Empirical Use. J. Exp. Bot. 10(2): 290–301. doi: 10.1093/jxb/10.2.290.

Richter, D.D., and D. Markewitz. 2001. Understanding soil change: soil sustainability over millennia, centuries, and decades. Cambridge University Press.

Riley, S.J. 1999. Index that quantifies topographic heterogeneity. Intermt. J. Sci. 5(1–4): 23–27.

Robarge, W.P., and I.J. Fernandez. 1987. Quality assurance methods manual for laboratory analytical techniques. US Environmental Protection Agency, US Department of Agriculture, Forest Service.

Robin, X., N. Turck, A. Hainard, N. Tiberti, F. Lisacek, et al. 2011. pROC: an open–source package for R and S+ to analyze and compare ROC curves. BMC Bioinformatics 22(1).

Ross, D.S., S.W. Bailey, R.D. Briggs, J. Curry, I.J. Fernandez, et al. 2015. Inter-laboratory variation in the chemical analysis of acidic forest soil reference samples from eastern North America. Ecosphere 6(5): 1–22. doi: 10.1890/ES14-00209.1.

Sandvoss, M., B. McClymond, and C. Farnden. 2005. User's Guide to the Vegetation Resources Inventory (technical report). Government of British Columbia.

Sauer, D., H. Sponagel, M. Sommer, L. Giani, R. Jahn, et al. 2007. Podzol: Soil of the Year 2007. A review on its genesis, occurrence, and functions. J. Plant Nutr. Soil Sci. 170(5): 581–597. doi: 10.1002/jpln.200700135.

Scarpone, C., M.G. Schmidt, C.E. Bulmer, and A. Knudby. 2017. Semi-automated classification of exposed bedrock cover in British Columbia's Southern Mountains using a Random Forest approach. Geomorphology 285: 214–224. doi: 10.1016/j.geomorph.2017.02.013.

Schaetzl, R.J. 2002. A Spodosol-Entisol Transition in Northern Michigan. Soil Sci. Soc. Am. J. 66(4): 1272–1284. doi: 10.2136/sssaj2002.1272.

Schaetzl, R.J., and W. Harris. 2011. Spodosols. Handb. Soil Sci. 2nd Ed CRC Press N. Y.: 33–113.

Schaetzl, R.J., and M.L. Thompson. 2015. Soils: genesis and geomorphology. Cambridge University Press.

Schoeneberger, P.J. 2012. Field book for describing and sampling soils. Natural Resources Conservation Service, National Soil Survey Center, Lincoln, NE.

Schoenholtz, S.H., H.V. Miegroet, and J.A. Burger. 2000. A review of chemical and physical properties as indicators of forest soil quality: challenges and opportunities. For. Ecol. Manag. 138(1): 335–356. doi: 10.1016/S0378-1127(00)00423-0.

Schwarz, P.A., T.J. Fahey, C.W. Martin, T.G. Siccama, and A. Bailey. 2001. Structure and composition of three northern hardwood–conifer forests with differing disturbance histories. For. Ecol. Manag. 144(1): 201–212. doi: 10.1016/S0378-1127(00)00371-6.

Seibert, J., and B.L. McGlynn. 2007. A new triangular multiple flow direction algorithm for computing upslope areas from gridded digital elevation models. Water Resour. Res. 43(4). doi: 10.1029/2006WR005128.

Shi, X., R. Long, R. Dekett, and J. Philippe. 2009. Integrating Different Types of Knowledge for Digital Soil Mapping. Soil Sci. Soc. Am. J. 73(5): 1682–1692. doi: 10.2136/sssaj2007.0158.

Siccama, T.G., T.J. Fahey, C.E. Johnson, T.W. Sherry, E.G. Denny, et al. 2007. Population and biomass dynamics of trees in a northern hardwood forest at Hubbard Brook. Can. J. For. Res. 37(4): 737–749. doi: 10.1139/X06-261.

Skovsgaard, J.P., and J.K. Vanclay. 2008. Forest site productivity: a review of the evolution of dendrometric concepts for even-aged stands. For. Int. J. For. Res. 81(1): 13–31. doi: 10.1093/forestry/cpm041.

Soil Survey Staff. 2014. Keys to Soil Taxonomy. 12th ed. Department of Agriculture: Natural Resources Conservation Service.

Sommer, M. 2006. Influence of soil pattern on matter transport in and from terrestrial biogeosystems—A new concept for landscape pedology. Geoderma 133(1): 107–123. doi: 10.1016/j.geoderma.2006.03.040.

Sommer, M., D. Halm, C. Geisinger, I. Andruschkewitsch, M. Zarei, et al. 2001. Lateral podzolization in a sandstone catchment. Geoderma 103(3): 231–247. doi: 10.1016/S0016-7061(01)00018-0.

Sommer, M., D. Halm, U. Weller, M. Zarei, and K. Stahr. 2000. Lateral Podzolization in a Granite Landscape. 64(4): 1434–1442. doi: 10.2136/sssaj2000.6441434x.

Sørensen, R., and J. Seibert. 2007. Effects of DEM resolution on the calculation of topographical indices: TWI and its components. J. Hydrol. 347(1): 79–89. doi: 10.1016/j.jhydrol.2007.09.001.

Stage, A.R. 1976. An Expression for the Effect of Aspect, Slope, and Habitat Type on Tree Growth. For. Sci. 22(4): 457–460. doi: 10.1093/forestscience/22.4.457.

Su, J., and E. Bork. 2006. Influence of vegetation, slope, and lidar sampling angle on DEM accuracy. Photogramm. Eng. Remote Sens. 72(11): 1265–1274. doi: 10.14358/PERS.72.11.1265.

Tesfa, T.K., D.G. Tarboton, D.G. Chandler, and J.P. McNamara. 2009. Modeling soil depth from topographic and land cover attributes. Water Resour. Res. 45(10). doi: 10.1029/2008WR007474.

Travis, M.R., G.H. Elsner, W.D. Iverson, and C.G. Johnson. 1975. VIEWIT: computation of seen areas, slope, and aspect for land-use planning. Gen Tech Rep PSW-GTR-11 Berkeley CA Pac. Southwest Res. Stn. For. Serv. US Dep. Agric. 70 P 011. http://www.fs.usda.gov/treesearch/pubs/27276 (accessed 26 October 2018).

U.S. Forest Service. 2005. White Mountain National Forest: Land and Resource Management Plan. http://www.fs.fed.us/r9/forests/ white mountain/ (accessed 20 May 2018).

U.S. Forest Service. Natural Resource Manager (NRM). Nat. Resour. Manag. https://www.fs.fed.us/nrm/ (accessed 20 May 2018).

Vaze, J., J. Teng, and G. Spencer. 2010. Impact of DEM accuracy and resolution on topographic indices. Environ. Model. Softw. 25(10): 1086–1098. doi: 10.1016/j.envsoft.2010.03.014.

Wang, L., and H. Liu. 2006. An efficient method for identifying and filling surface depressions in digital elevation models for hydrologic analysis and modelling. Int. J. Geogr. Inf. Sci. 20(2): 193–213. doi: 10.1080/13658810500433453.

Warby, R.A.F., C.E. Johnson, and C.T. Driscoll. 2009. Continuing Acidification of Organic Soils across the Northeastern USA: 1984–2001. Soil Sci. Soc. Am. J. 73(1): 274–284. doi: 10.2136/sssaj2007.0016.

Weiskittel, A., P. Gould, and H. Temesgen. 2009. Sources of variation in the self-thinning boundary line for three species with varying levels of shade tolerance. For. Sci. 55(1): 84–93.

Wilde, S.A. 1958. Forest soils. Chronica Botanica Co., Waltham, Mass.

Wood, S.N. 2004. Stable and Efficient Multiple Smoothing Parameter Estimation for Generalized Additive Models. J. Am. Stat. Assoc. 99(467): 673–686. doi: 10.1198/016214504000000980.

Woodall, C.W., P.D. Miles, and J.S. Vissage. 2005. Determining maximum stand density index in mixed species stands for strategic-scale stocking assessments. For. Ecol. Manag. 216(1): 367–377. doi: 10.1016/j.foreco.2005.05.050.

Yanai, R.D., T.G. Siccama, M.A. Arthur, C.A. Federer, and A.J. Friedland. 1999. Accumulation and Depletion of Base Cations in Forest Floors in the Northeastern United States. Ecology 80(8): 2774–2787. doi: 10.2307/177257.

Zeide, B. 2005. How to measure stand density. Trees 19(1): 1–14. doi: 10.1007/s00468-004-0343-x.

Zevenbergen, L.W., and C.R. Thorne. 1987. Quantitative analysis of land surface topography. Earth Surf. Process. Landf. 12(1): 47–56.

Zhu, A.X., B. Hudson, J. Burt, K. Lubich, and D. Simonson. 2001. Soil Mapping Using GIS, Expert Knowledge, and Fuzzy Logic. Soil Sci. Soc. Am. J. 65(5): 1463. doi: 10.2136/sssaj2001.6551463x.

APPENDIX

Figure S2.1: WAMMO watershed buffered by 200 meters depicting predicted bedrock outcrop-shallow soil locations in dark grey. Manual delineation of bedrock-controlled areas is depicted by lighter grey polygons. Overall agreement on bedrock occurrence is high, however, predicted bedrock outcrop-shallow soils suggest higher presence of small pockets in valley bottoms.

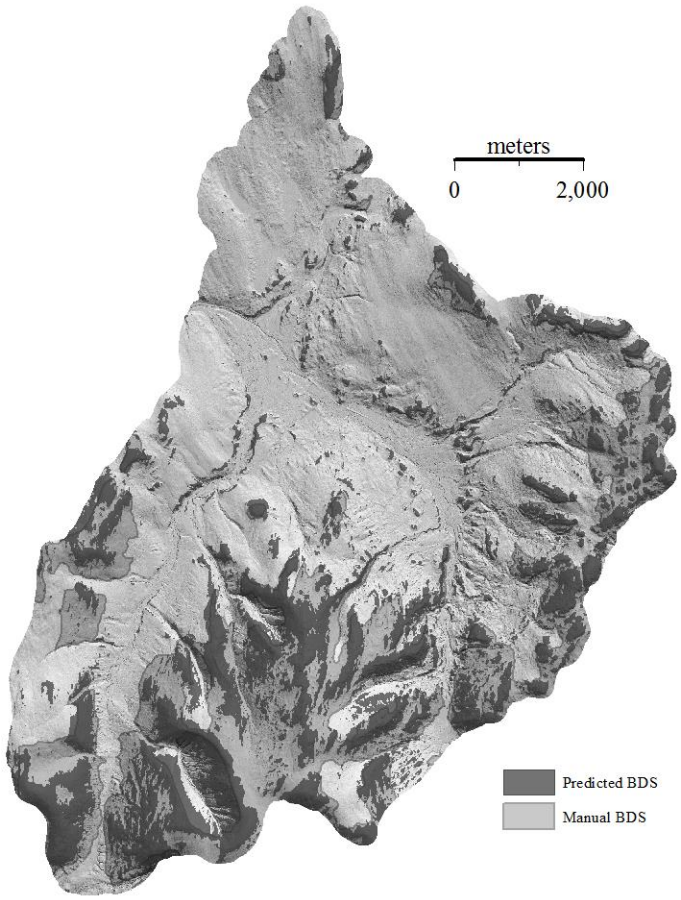

Supplemental Table 4.1: Plot location names, ID, elevation (m), aspect (°), plan curvature, slope (%), dominant hydrological pathway influencing soil formation, slope position, and landform.

Name	ID	Elev	Aspect	Plan	Slope	Hydro†	Slope position	Landform
Ames Brook 1	AB1	567	318	150	10	Lateral	Mid backslope	Nose
Bunga Jar 1	BJ1	430	3	221	17	Bimodal	Toe slope	Planar slope
Bunga Jar 2	BJ2	424	220	310	11	Bimodal	Lower backslope	Nose
Bunga Jar 3	BJ3	558	347	172	8	Vertical	Shoulder	Nose
Bald Ledge 1	BL1	533	221	295	13	Vertical	Upper backslope	Nose
Castle Trail 1	CT1	648	14	222	18	Lateral	Upper backslope	Nose
Castle Trail 2	CT2	633	33	204	23	Vertical	Mid backslope	Planar slope
Castle Trail 3	CT3	586	356	141	7	Lateral	Toe slope	Planar slope
Fox Brook 1	FX1	507	235	284	14	NA	Mid backslope	Foot slope
Fox Brook 2	FX2	489	304	293	9	Lateral	Toe slope	Planar slope
Fox Brook 3	FX3	616	112	193	14	Vertical	Mid backslope	Planar slope
Fox Brook 4	FX4	708	341	74	15	Lateral	Shoulder	Spur foot
Glencliff 1	GC1	646	310	55	11	Bimodal	Mid backslope	Hollow
Glencliff 2	GC2	683	318	60	12	Vertical	Mid backslope	Nose
Glencliff 3	GC3	472	247	330	3	Bimodal	Toe slope	Nose
Greeley Brook 1	GR1	603	208	227	5	Lateral	Mid backslope	Planar slope
Greeley Brook 2	GR2	637	166	262	10	Vertical	Shoulder	Spur foot
Greeley Brook 3	GR3	567	235	327	9	Lateral	Toe slope	Foot slope
Haystack Mtn 2	HM2	741	357	285	21	Lateral	Lower backslope	Planar slope
Jefferson Notch 2	JN2	638	336	80	20	Vertical	Mid backslope	Nose
Lafayette Brook 1	LB1	646	32	277	13	Vertical	Mid backslope	Spur
Lafayette Brook 2	LB2	500	312	35	5	Vertical	Toe slope	Hollow
Lafayette Brook 3	LB3	695	22	273	2	Bimodal	Upper backslope	Nose
Morrison Brook 1	MB1	411	242	118	13	Bimodal	Backslope	Planar slope
Morrison Brook 2	MB2	468	280	0	25	Vertical	Backslope	Nose
Morrison Brook 3	MB3	390	225	344	13	Vertical	Lower backslope	Planar slope
Miles Knob 1	MK1	508	275	230	22	Vertical	Upper backslope	Planar slope
Miles Knob 2	MK2	317	160	210	16	Vertical	Mid backslope	Nose
Moat Mtn. 1	MO1	248	80	172	10	Vertical	Mid backslope	Planar slope
Pond of Safety 1	PS1	684	295	190	17	Lateral	Mid backslope	Nose
Rattle River 1	RR1	421	26	120	16	Vertical	Mid backslope	Hollow
Rattle River 2	RR2	381	8	281	8	Vertical	Upper backslope	Nose
Rattle River 3	RR3	404	270	345	11	Vertical	Mid backslope	Planar slope
Shingle Pond 1	SP1	555	135	245	8	Vertical	Mid backslope	Planar slope
Shingle Pond 2	SP2	518	184	270	6	Vertical	Mid backslope	Planar slope
Stinson Mtn. 1	ST1	515	201	264	22	Vertical	Upper backslope	Nose
Wildwood 1	WW1	499	183	275	6	Vertical	Backslope	Planar slope
Wildwood 2	WW2	634	219	308	18	Vertical	Mid backslope	Planar slope

†Dominant hydrologic pathway influencing soil formation

Supplemental Figure S4.1: pH vertical distributions by depth (cm) for 39 sites. Solid black lines represent 2001-02 sampling year and dashed grey lines represent 2014 sampling year.

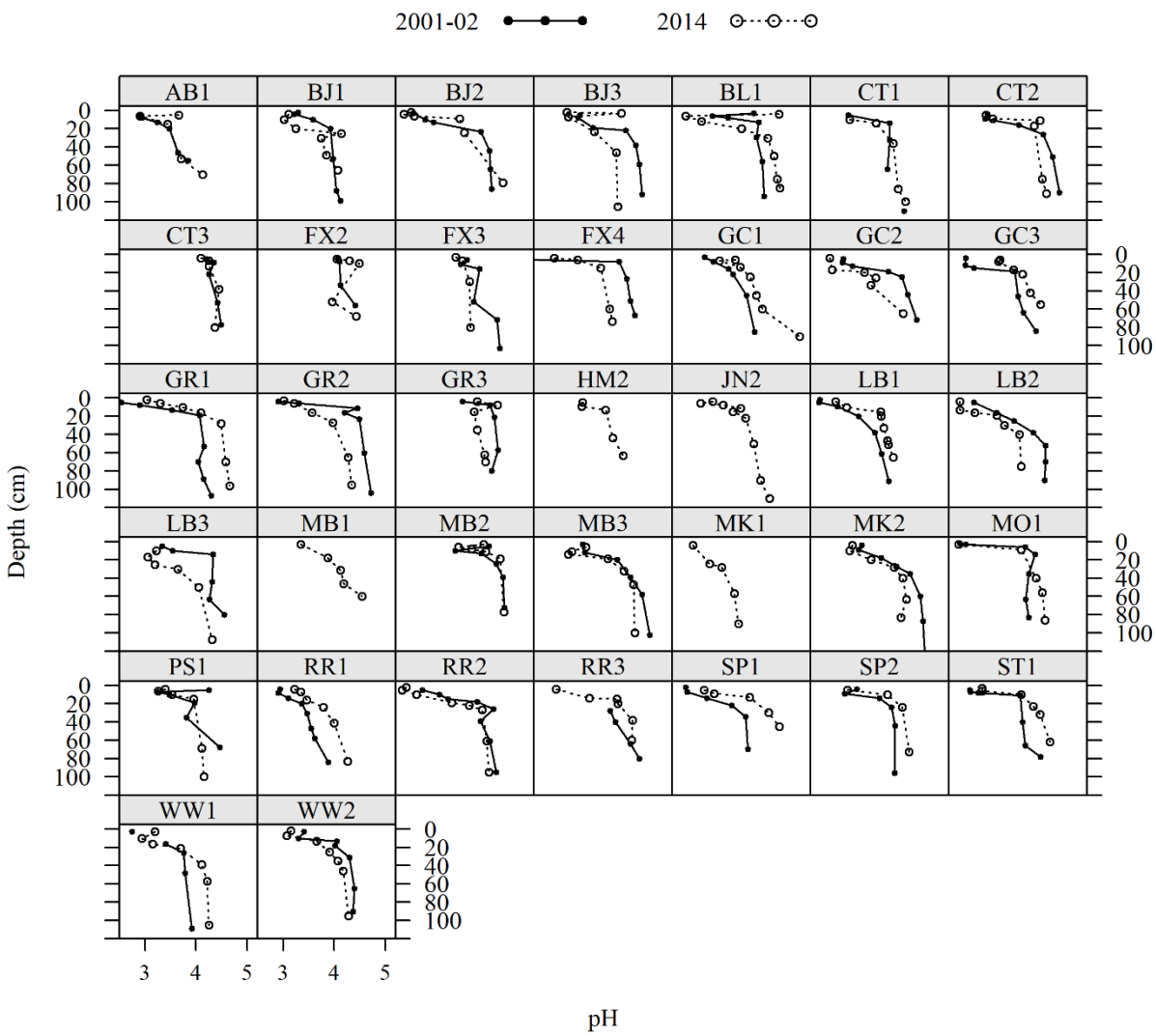

Supplemental Figure S4.2: Exchangeable Al (cmolc kg^{-1}) vertical distributions by depth (cm) of for 39 sites. Solid black lines represent 2001-02 sampling year and dashed grey lines represent 2014 sampling year.